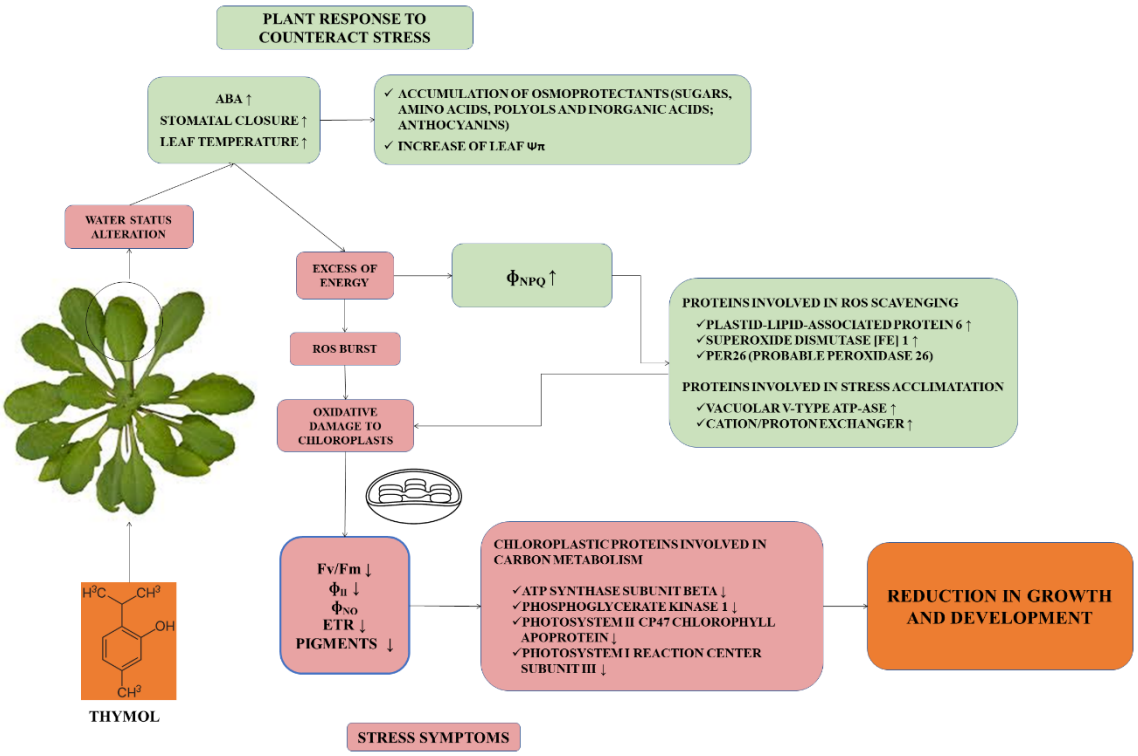
PLANT RESPONSE TO COUNTERACT STRESS
ABA ↑
STOMATAL CLOSURE ↑
LEAF TEMPERATURE ↑
✓ ACCUMULATION OF OSMOPROTECTANTS (SUGARS, AMINO ACIDS, POLYOLS AND INORGANIC ACIDS; ANTHOCYANINS)
✓ INCREASE OF LEAF Ψπ
WATER STATUS ALTERATION
EXCESS OF ENERGY
ΦNPQ ↑
ROS BURST
OXIDATIVE DAMAGE TO CHLOROPLASTS
PROTEINS INVOLVED IN ROS SCAVENGING
✓PLASTID-LIPID-ASSOCIATED PROTEIN 6 ↑
✓SUPEROXIDE DISMUTASE [FE] 1 ↑
✓PER26 (PROBABLE PEROXIDASE 26)
PROTEINS INVOLVED IN STRESS ACCLIMATATION
✓VACUOLAR V-TYPE ATP-ASE ↑
✓CATION/PROTON EXCHANGER ↑
Fv/Fm ↓
ΦII ↓
ΦNO
ETR ↓
PIGMENTS ↓
CHLOROPLASTIC PROTEINS INVOLVED IN CARBON METABOLISM
✓ATP SYNTHASE SUBUNIT BETA ↓
✓PHOSPHOGLYCERATE KINASE 1 ↓
✓PHOTOSYSTEM II CP47 CHLOROPHYLL APOPROTEIN ↓
✓PHOTOSYSTEM I REACTION CENTER SUBUNIT III ↓
REDUCTION IN GROWTH AND DEVELOPMENT
H3C
CH3
OH
CH3
THYMOL
STRESS SYMPTOMS

Metabolomic, proteomic and physiological insights into the potential mode of action of thymol, a phytotoxic natural monoterpenoid phenol

Fabrizio Araniti[1*], Begoña Miras-Moreno[2], Luigi Lucini[2], Marco Landi[3], Maria Rosa Abenavoli[1]

[1]Department AGRARIA, University Mediterranea of Reggio Calabria, – Località Feo di Vito, SNC I-89124 Reggio Calabria RC, Italy

[2]Department for Sustainable Food Process, Università Cattolica del Sacro Cuore, via Emilia parmense 84, 29122 Piacenza, Italy

[3]Department of Agriculture, Food and Environment, University of Pisa, Pisa, Italy

*Corresponding author:
fabrizio.araniti@unirc.it
Department AGRARIA,
University Mediterranea of Reggio Calabria,
Località Feo di Vito,
SNC I-89124
Reggio Calabria RC,
Italy

Short title: *The phytotoxic effect of thymol on adult plants of A. thaliana*

Abstract

Thymol is a natural phenolic monoterpene widely produced by different species belonging to the *Labiateae* family. Although the thymol phytotoxicity is well known, the knowledge of its potential toxic mechanism is still limited. In this regard, the model species *Arabidopsis thaliana* was treated for 16 days by sub-irrigation with 300 μM of thymol. The results confirmed the high phytotoxic potential of this phenolic compound, which caused a reduction in plant growth and development. Thymol induced a water status alteration accompanied by an increase in ABA content and stomatal closure. Furthermore, leaves appeared necrotic in the margins and their temperature rinsed. The increase in H_2O_2 content suggested an oxidative stress experienced by treated plants. Both metabolomic and proteomic analysis confirmed this hypothesis showing a strong increase in osmoprotectants content, such as galactinol and proline, and a significant up-accumulation of proteins involved in ROS detoxification. Furthermore, the down-accumulation of proteins and pigments involved in the photosynthetic machinery, the increase in light sensitivity and the lower PSII efficiency well indicated a reduction in photosynthetic activity. Overall, we can postulate that thymol-induced phytotoxicity could be related to a combined osmotic and oxidative stress that resulted in reduced plant development.

Keywords: specialized metabolites; natural herbicide; oxidative stress; photosynthesis; photosystem II; plant water status.

1. Introduction

Weeds are still the most important pest problem in fields, since they compete with crops for water and nutrient resources reducing their yields and quality, and causing great losses to agriculture (Zimdahl, 2018). Nowadays, to maximize the agricultural efficiency, weed control mainly occurs using chemical herbicides (Harrison and Loux, 2017). However, the negative impact of these synthetic compounds on the environment and the human health together with the rapid increase of weeds resistance has made more insistent and stringent to develop alternative methods for weed control (Busi et al., 2018; Westwood et al., 2018). The identification of natural or natural-like molecules, with new modes of action, could be a valid alternative as new bio-herbicides or templates for new synthetic herbicides in a sustainable agriculture (Busi et al., 2018; Duke et al., 2018). Among these, essential oils (EOs) and their constituents, produced by plants, are very interesting compounds which activity has already been proved in agriculture for their fungicidal, insecticidal and nematicidal activity (Arancibia et al., 2017; Chen et al., 2019; Isman et al., 2019). The EOs have been frequently reported for their positive (interesting) effect on weed control according to their allelopathic features (Alipour et al., 2019; Benvenuti et al., 2017; Nikolova et al., 2018). A large number of terpenoids has been identified in EOs that are involved in plant-plant interactions, inhibiting growth and development of many crops and weeds through multiple physiological effects (Araniti et al., 2017b; Landi et al., 2020). Among these, carvacrol, farnesene, citral, *trans*-caryophyllene and thymol are phytotoxic terpenoids with a promising herbicidal activity (Araniti et al., 2016; Araniti et al., 2017a; Araniti et al., 2017c; Araniti et al., 2018; de Assis Alves et al., 2018; Graña et al., 2013).

In particular, thymol is a natural occurring phenol monoterpene widely distributed in the plant kingdom, being a major constituent of EOs, together its isomer (Naghdi Badi et al., 2017). Nowadays, thymol has a wide range of functional roles in drug, food and cosmetic industry due to its potential antimicrobial, antioxidant, anticarcinogenesis and anti-inflammatory activities (Gursul et al., 2019; Li et al., 2017; Salehi et al., 2018; Pivetta et al., 2018).

In plants, thymol completely inhibited seed germination and seedlings growth of Johnson grass (*Sorghum halepense* L.) (Matković et al., 2018), *Amaranthus retroflexus*, *Chenopodium album* and *Rumex crispus*, showing a potent phytotoxic effect (Kordali et al., 2008). The application of several monoterpene compounds, such as thymol, on maize roots induced a modification of the sterol proportion, which changed unsaturation of fatty acids, increasing unsaturated phospholipids percentage and consequently the membrane permeability (Zunino et al., 2005). Recently, thymol displayed a clastogenic and aneugenic action, resulting in damage to the DNA and the mitotic spindle in both eudicots (lettuce) and monocots (sorghum) and exhibiting a strong phytotoxic and cytotoxic activity (de Assis Alves et al., 2018). In particular, the thymoxyacetic acid, obtained from thymol by

acidification, showed a toxicity similar to that of the commercial herbicide 2,4-D, being more pronounced in *L. sativa* (eudicot) than in *S. bicolor* (monocot) (de Assis Alves et al., 2018). Furthermore, Nasrollahi et al. (2018) demonstrated that thymol decreased photosynthetic rate and chlorophyll fluorescence in lettuce treated plants, increasing, in contrast, photochemical efficiency of photosystem II, proline content and several antioxidant enzymes.

Despite the large evidences regarding its wide biological activity, no clues are given concerning potential mode of action (MOA) of thymol on plants, fundamental for its use in agriculture. Noteworthy, thymol has been listed as a potential candidate to be developed as safe agrochemical based on US Environmental Protection Agency of the United States assessments (USEPA/IRIS, 2014).

Due to the intrinsic complexity to understand the MOA, different approaches are required in several scientific fields. In recent years, *–omics* techniques, such as transcriptomic, proteomic and metabolomics together with physiological, biochemical and/or molecular approaches could lead to the understanding of the impact of natural toxins and their MOA on plant metabolism.

In this respect, in the present paper the effects of thymol and its MOA on adult plants of *Arabidopsis thaliana*, through an integrated -omics (metabolomic and proteomic) and physiological approach, have been proposed.

2. Materials and methods

2.1 Dose-response curve: the phytotoxic effect of thymol on A. thaliana

Arabidopsis thaliana L. (Heyn.) ecotype Columbia (Col-0) seeds were sterilized and vernalized as previously described by Araniti et al (2013). After sterilization, seeds were sown in Petri dishes (10 x 10 cm) containing agar medium (0.8%) enriched with macro- and micronutrients (Murashige – Skoog basal salt; Sigma-Aldrich) and sucrose (1%), pH 6.0. Sown plates were placed, in a vertical position, in a growth chamber, at 22 °C ± 2 °C, 8 / 16 h, light (90 mol m^{-2} s^{-1}) / darkness photoperiod, and 55% relative humidity. Immediately after germination, 10 seedlings, selected for uniform size, were transplanted on Petri dishes and treated with 0, 50, 100, 200, 400, 800 and 1200 µM thymol, for 14 days. At the end of the treatment, a bunch of 10 seedlings, per treatment and replicate, was collected and fresh weight (FW) of seedlings was evaluated. Raw data where then fitted through non-linear regression to identify the ED_{50} parameter (the concentration of thymol which cause the 50% of FW inhibition) on which to focus the next experiments.

2.2 The phytotoxic effect of thymol on A. thaliana adult plants

Experiments on adult plants have been carried out as previously reported by Araniti et al. (2018) with some modifications. Uniform seedlings of *Arabidopsis thaliana* L. (Heyn.) Col-0 seedlings (30 per treatment, 14 days old), obtained in agar plates, as previously reported, were individually transplanted into pots (6 x 6 x 8 cm) containing Perlite (Agrilit 3), previously sterilized and moistened with half-strength Hoagland nutrient solution (pH 6.0). Transplanted seedlings were allowed to establish for 7 days and during which they were sub-irrigated every other day with a same nutrient solution. Thymol treatment began when plants were 3 weeks old. Thymol was solubilized in EtOH (0.1%) and diluted in half-strength Hoagland solution to reach final concentrations: 0 µM (control) and 300 µM. Thymol solutions were then applied in plants (3 weeks old), through sub-irrigation (25 ml/pot) every other day, for 16 days. EtOH 0.1% was added in the control solution.

2.3 Chlorophyll a fluorescence and pigments content

Chlorophyll *a* fluorescence emitted by adult plants of Arabidopsis treated with thymol was determined as previously described by Martínez-Peñalver et al. (2011) using the Maxi-Imaging-PAM Chlorophyll Fluorescence System fluorometer (Walz, Effeltrich, Germany). The following parameters were recorded every 2 d during 16 days of treatment: the maximum PSII efficiency in dark adapted leaves (F_v/F_m), the effective photochemical quantum yield of photosystem II (ϕ_{II}), the apparent electron transport rate (ETR), the quantum yield of light-induced nonphotochemical quenching (ϕ_{NPQ}), chlorophyll a fluorescence (ϕ_{NO}) and the fraction of the open photosystem II reaction centers (q_L). The photosynthetic response was monitored for 5 min, and fifteen measurements were obtained for each parameter at each measuring time, which output was a kinetic plot for each parameter along time. At the end of the experiment the integral value of the kinetic plot area for each replication, time point and parameter was calculated and reported on the graphs (Graña et al., 2013).

Chlorophyll *a*, chlorophyll *b* and carotenoids were quantified as previously reported by Araniti et al. (2017c). In particular, 100 mg of plant material, for each replicate and treatment, were extracted with methanol (1.5 ml) and then centrifuged at 170 g for 5 min. Subsequently, 500 µl of supernatant were diluted with 500 µl of methanol and sample absorbance was read at 470, 653, 666 and 750 nm. Pigment content, quantified using Wellburn's equations (Wellburn, 1994), was calculated as µg / g of DW and expressed as % compared to the control.

Anthocyanins were extracted from 0.2 g of leaf tissue previously grounded in liquid nitrogen. Samples, suspended in 1 mL water, were centrifuged at 18,000 g for 10 min. The supernatant was diluted with 0.4 M sodium acetate at pH 4.5 and 25 mM potassium chloride at pH 1.0, and centrifuged

once again. Total monomeric anthocyanins were measured by recording the A_{520} as outlined in Giusti and Wrolstad (2001).

2.4 Leaf temperature, stomatal density and size

Variations in leaf temperature were evaluated using a thermocamera (FLIR T640bx). Images were then analyzed using the Flir Tool software, which allowed measuring the temperature gradient from the leaf base (LV) till the distal part of the lamina (LB).

Immediately, after leaf detaching, both stomatal density (number of stomata per unit leaf area) and size (length between the junctions of the guard cells at each end of the stomata) were evaluated on untreated and treated plants using an epifluorescence microscope system (Olympus bx53) and expressed as percentage compared to the control (Malone et al., 1993; Radoglou and Jarvis, 1990; Xu et al., 2008).

2.5 Fresh weight (FW), dry weight (DW), DW/FW ratio, leaf number and area, leaf relative water content (RWC), leaf osmotic potential [Ψ (π)] and leaf membrane stability index [MSI (%)]

At the end of the experiment, a pool of four rosettes (biological sample), for each treatment and replicate, was collected and their FW, leaf number and area were evaluated. In particular, leaf area was quantified using the open source software ImageJ (Image Processing and Analysis in Java). Successively, plant samples were hoven dried at 60 °C to determine the DW and to calculate the DW/FW ratio.

Leaf relative water content (RWC) was estimated as previously reported by González and González-Vilar (2001). One leaf blade for each replicate was weighted (FW) and incubated in 15 ml of ultrapure water for 24 h at 4°C. After incubation, leaves were blotted and weighted to get the turgid weight (TW). Successively, leaf samples were oven dried and newly weighted (DW). FW, TW, and DW were used to evaluate the RWC parameter using the following formula:

$$\mathbf{RWC = [(FW - DW)/ (TW - DW)] * 100}$$

For the Ψπ leaf evaluation, four leaves, per treatment and replication, were collected and frozen at -20 °C. After 24 hours, defrosted leaves were squeezed into a syringe taking care to eliminate the first drop. The remaining extracts were collected in vials and their Ψπ was measured with a cryoscopic osmometer (Osmomat 030, Gonatec) (González, 2001; Araniti et al., 2018). The Ψπ leaf was expressed in mega pascal (MPa).

The MSI was determined indirectly as reported by Sairam et al. (2002). Leaf discs with uniform size (1cm Ø) were transferred in tubes containing 10 ml of ultrapure water. They were then heated at 30°C for 30 minutes and successively the electrical conductivity was measured (C1). Samples were then transferred in a bath at 100°C for 30 minutes, were then cooled on ice and the electric conductivity was again measured (C2). The MSI index was calculated using the following formula:

$$\mathbf{MSI\ (\%) = (1- C_1/C_2) * 100}$$ (Sairam, 2002)

2.6 Relative quantification of abscisic acid through GC-MS

Arabidopsis rosettes were cut, deeply frozen in liquid nitrogen, powdered and transferred in a 2 ml centrifuge tube (0.1 ± 0.002 g), for each treatment and replicate. Sample extraction and derivatisation were carried out as previously described by Rawlinson et al. (2015), with some modifications. To the powdered frozen samples, 20 µl of indole propionic acid (20 mg/ml) were added as internal recovery standard. Successively, 200 µl of NaOH (1 % w/v), 147 µl of MeOH and 34 µl of pyridine were added to samples, and vortexed for 40 sec. To the extracted samples were added 20 µl of methyl chloroformate and newly vortexed for 30 sec. This step was repeated two times. To samples were added 400 µl of chloroform, shaken for 10 sec., and 400 µl of $NaHCO_3$ solution (50 mM). Samples were shaken for 20 sec and immediately centrifuged (22000 g) for 1 min. The organic fraction was collected, dispensed in 2 ml centrifuge tubes and the aqueous residues were eliminated using anhydrous Na_2SO_4. One hundred µl of organic fraction were used for the GC-MS analysis, which was carried out using a GC-MS single quadrupole apparatus equipped with a TG-5MS capillary column. Helium was used as gas carrier with a flow rate of 1 ml/min. Injector and transfer line were settled at 250°C and 270°C, respectively. Three µl of sample were injected with a 35 psi pressure pulse, which was held for 1 min. The following temperatures were programmed: isocratic for 1 minute at 40°C, from 40°C to 320°C with a rate of 20°C×min, then isocratic for 2 min 320°C. The ion source was settled at 200°C and the solvent delay was 4.5 min. Mass spectra were recorded in electronic impact (EI) mode at 70 eV, scanning at 50–400 m/z range for selection of appropriate EI mass fragments for each analyte. Then, the MS was run in selected ion monitoring (SIM) using 1 quantifier ion (*m/z*) and two qualifiers (*m/z*) for ABA-methyl ester the ions 190 (quantifier), 162 and 134 (qualifiers) were used. The ABA identification was carried out comparing the relative retention time and mass spectra of molecule with pure standards derivatized, as previously described, and with the commercial libraries (NIST 2005, Wiley 7.0 etc.). The ABA content was

previously normalized on the internal standard amount (indole propionic acid) and quantified using a standard curve built with ABA derivatized pure standard.

2.7 In-situ semi-quantitative determination of H_2O_2, lipid peroxidation, and protein content

The H_2O_2 was determined following the method proposed by van Acker et al. (2000) successively modified by Sánchez-Moreiras et al. (2011). Four fully expanded leaves were cut, infiltrated under vacuum and incubated in dark condition for 8 h in the 3,3'-diaminobenzidine (DAB) (1 mg mL^{-1}) solution (pH 3.8). After incubation, leaves (5 leaves for each treatment and replicate) were exposed to light for 30 min and successively pigments were removed using an ethanol : acetic acid (1:1 v/v) solution. The percentage of stained leaf area was evaluated using the image analysis software Image ProPlus v.6.0 (Media Cybernetics Inc., Bethesda, MD, USA).

Lipid peroxidation was quantified as previously described by Hodges et al. (1999), using 100 mg of fresh plant material, obtained from a pool of four full rosettes, for each treatment and replicate. The MDA equivalents were calculated using the equations proposed by Hodges et al. (1999), corrected by Landi (2017), and then expressed in percentage compared to the control.

Total protein content of Arabidopsis leaves was determined according to the Bradford (1976) protocol, using bovine serum albumin as standard. Total protein content, calculated as µg per gram of DW, was expressed in percentage compared to the control.

2.8 Extraction, identification and quantification of primary metabolites in Arabidopsis leaves

Plant materials (a pool of four full rosettes, for each treatment and replicate) were collected and immediately snap frozen in liquid nitrogen to quench the metabolism. Freshly homogenized (100 mg) plant material were obtained for each biological sample and replicates.

Extraction was done by adding 1400 µl of methanol (at -20°C) to samples and vortexed for 30 s after addition of 60 µl ribitol (0.2 mg/ml stock in d H_2O) as an internal quantitative standard. Samples were then transferred in a thermomixer at 70°C, shaken for 10 min (950 rpm), and centrifuged for 10 min at 11000 g. The supernatants were collected and transferred to glass vials where 750 µl $CHCl_3$ (-20°C) and 1500 µl ddH_2O (4°C) were sequentially added. All the samples were vortexed for 10 s and then centrifuged for 15 min at 2200 g. Upper polar phase (150 µl), for each treatment and replicate, was collected, transferred to a 1.5 ml tube and dried in a vacuum concentrator without heating. Before freezing and storing at -80° C, the tubes were filled with argon and placed in a plastic bag with silica beads (for avoiding moisture and hydration during short-term storage). Before derivatization, stored samples were placed in a vacuum concentrator for 30 minutes to eliminate any

trace of humidity. Then, 40 µl of methoxyamine hydrochloride (20 mg/ml in pyridine) were added to the dried samples and incubated for 2 h in a Thermomixer (950 rpm) at 37°C. Methoxyaminated samples were then silylated by adding 70 µl of MSTFA (N,O-bis-trimetilsilil-trifluoroacetamide) to the aliquots. Samples were further shaken for 30 min at 37°C. Derivatized samples (110 µl) were then transferred into glass vials suitable for the GC/MS autosampler. For analysis injector and source were settled at 250°C and 260°C temperature, respectively. One µl of sample was injected in splitless mode with a flow of 1ml/min using the following programmed temperature: isothermal 5 min at 70 °C followed by a 5°C/ min ramp to 350 °C and a final 5 min heating at 330°C. Mass spectra were recorded in electronic impact (EI) mode at 70 eV, scanning at 45–500 m/z range, solvent delay 9 minutes.

In addition to samples, an *n*-hydrocarbons mixture (alkane calibration standard all even C8-C40, Sigma Aldrich, Italy) and blank samples were separately injected. The alkane standards were used for Retention Index calculation, whereas the blank sample for removing features based on blank information (Lisec et al., 2006).

The MS DIAL with open source public available EI spectra libraries were used for raw peaks extraction and the data baseline filtering and calibration of the baseline, peak alignment, deconvolution analysis, peak identification and integration of the peak height essentially followed as described (Tsugawa et al., 2015). An average peak width of 20 scan and minimum peak height of 1000 amplitudes were applied for peak detection, and sigma window value of 0.5, EI spectra cut-off of 10 amplitudes were implemented for deconvolution. For identification, 0.5 min of the retention time tolerance, 0.5 Da of the m/z tolerance, 60% of the EI similarity cut-off, and 80% of the identification score cut-off were settled. In the alignment parameters setting process, both the retention time tolerance and retention time factor were 0.5 min. For, MS-DIAL data annotations we used publicly available libraries. Compound identification was based on the mass spectral pattern as compared to EI spectral libraries such as the NIST Mass Spectral Reference Library (NIST14/2014), the MSRI spectral libraries from Golm Metabolome Database (Kopka et al., 2005) available from Max-Planck-Institute for Plant Physiology, Golm, Germany, MassBank (Horai et al., 2010), the MoNA (Mass Bank of North America).

2.9 Proteomic analysis

Proteomic analysis was performed on an aliquot of samples used for metabolomics following the method reported by Salehi et al. (2018). Briefly, proteins were extracted in phenol (buffered with Tris HCl, pH 8.0, Sigma, St.Louis, MO, USA), precipitated in five volumes of 0.1M ammonium acetate in cold methanol, reduced and alkylated, then digested overnight using porcine trypsin (Promega,

Madison, CA, USA). Peptides were analyzed by shotgun data-dependent MS/MS using a 1260 nano-LC Chip Cube source coupled to a 6550 iFunnel quadrupole-time-of-flight mass spectrometer (both from Agilent Technologies, Palo Alto, CA, USA). Peptides were analyzed through a 60 min water-acetonitrile gradient (with 0.1% HCOOH), using a chip made of a 40 nL enrichment column and a 150 mm separation column (Agilent Zorbax 300SB-C18, 5 µm). The elution gradient was designed from 3% to 90% acetonitrile at a flow of 0.6 µl min^{-1}. The data-dependent tandem mass spectrometric acquisition was set to 20 precursors per cycle (4 Hz, 300-1700 m/z) with positive polarity. Ramped collision energy was used for collision-induced decomposition, as a function of peptide charge.

Proteins inference was carried out in Spectrum Mill MS Proteomics Workbench (Rev B.04; Agilent Technologies) setting carbamidomethylation of cysteine as a fixed modification and allowing one missing cleavage per peptide. Mass tolerance was ± 10 ppm and ± 20 ppm for precursor and product ions, respectively. Search was conducted against the proteome of *A. thaliana* (Uniprot, downloaded January 2018); the database was concatenated with the reverse one. Autovalidation with a target 1% false discovery rate and label-free quantitation (protein summed peptide abundance), were also adopted.

2.10 Statistical analysis

A completely randomized design with four replications was applied in all the experiments except for chlorophyll *a* fluorescence that was replicated 3 times. Data were first checked for normality through the Kolmogorov-Smirnov test and then tested for homogeneity of variances with the Levene's test. Differences among treatments were statistically evaluated through t-test ($P \leq 0.05$). Differences among treatments in chlorophyll *a* fluorescence experiments were statistically evaluated by analysis of variance followed by Least Significant Difference tests (LSD) ($P \leq 0.05$).
The ED_{50} value was evaluated by a nonlinear regression model using a log-logistic function as reported by Beltz et al. (2005).

Metabolite concentrations were checked for integrity and missing values were replaced with a small positive value (the half of the minimum positive number detected in the data). Data were then normalized by the reference feature (ribitol), transformed through "Log normalization" (to make the metabolite concentration values more comparable among different compounds) and scaled through Pareto-Scaling (mean-centered and divided by the square root of standard deviation of each variable). Data were then classified through Principal Component Analysis (PCA), metabolite variations were presented and samples clustered through a heatmap. Differences between treatments were considered

significant when the $P \leq 0.05$ (Student's *t*-test). Metabolomic data handling were carried out using the software metaboanalyst 4.0 (Chong et al., 2018).

Proteomic data were elaborated using Mass Profiler Professional B.04 (Agilent Technologies), as previously reported (Bernardo et al., 2017). Briefly, data were Log2 normalized, baselined against the median of control and then an unsupervised hierarchical cluster analysis (distance: Euclidean; linkage rule: Ward's), based on fold-change heatmaps, was carried out to naively identify the relatedness/unrelatedness between treatments. Thereafter, the dataset was elaborated through Partial Least Squares Discriminant Analysis (PLS-DA), a multivariate supervised approach that allowed identifying the most discriminant proteins according to their weight in the PLS-DA prediction model (as resulted from the model Score Plot). A fold-change analysis (fold-change cut-off =3) was finally performed to describe the extent and direction of the accumulation.

The ontology of differentially accumulated proteins was finally investigated using the online tools agriGO 2.0 (Tian et al., 2017) and DAVID 6.8 (Sherman and Lempicki, 2009; Galperin and Cochrane, 2009) to summarize the biochemical processes involved in plant response to thymol.

3. RESULTS

3.1. Phytotoxic effect of thymol on A. thaliana

Thymol severely affected shoot growth of *A. thaliana* in a dose dependent manner. In particular, FW reduction was significantly evident already at 100 µM (25 %). Such reduction increased along with the increasing of thymol concentrations reaching 81% and 93% with 800 µM and 1200 µM treatments, respectively (Fig. 1).

The fitting of the dose response curve through non-linear regression allowed evaluating the ED_{50} parameters, which was 289.2 µM (Fig. 1).

3.2 Fresh weight (FW), dry weight (DW), DW/FW ratio, leaf number and area, leaf relative water content (RWC) and leaf osmotic potential (Ψπ)

Thymol treatment significantly altered all the morpho-physiological parameters evaluated. In particular both fresh and dry weight pointed out a 47% and 33% reduction, respectively. On the other hand, DW/FW ratio significantly increased (25%). At the same, plant growth inhibition was accompanied by a reduction of the leaf number, already observed after 4 days of treatment, a decrease of the leaf area (36%) and the RWC (69%), and an increase of the Ψπ (16%) (Ψπ is characterized by

negative value, so an increase of 16% means that the Ψπ in plants treated was a 16% more negative than control) (Fig. 2).

3.3 Lipid peroxidation, protein content, leaf membrane stability index [MSI (%)] and in-situ semi-quantitative determination of H_2O_2

In plants treated with thymol, an increment in lipid peroxidation (57%) accompanied by a reduction in total proteins (43%) and membrane stability (44%), were observed (Fig. 4). Moreover, in DAB stained leaves, a clear increment in H_2O_2 content was highlighted by the brownish leaves coloration (Fig. 3).

3.4 Leaf stomatal density and size, leaf temperature and ABA content

Plants treated with thymol pointed out an increment in ABA content (51%) accompanied by the stomatal closure and the reduction in both density (45%) and size (37%) (Fig. 4). Moreover, in plants treated an increment in temperature in all parts of leaf was observed, especially high in the peripheral areas of the blade decreasing toward the midrib and the petiole (Fig. 4).

3.5. Chlorophyll a fluorescence and pigment content

The chlorophyll *a* fluorescence monitoring pointed out a severe alteration of the photosynthetic machinery in thymol-treated adult plants. In particular, the parameters F_v/F_m (after 6 days of treatment), ϕ_{II} and ETR (after 8 days) were significantly reduced by treatment. On the contrary, ϕ_{NO} and ϕ_{NPQ} were significantly increased after eight days (Fig. 5).

Concerning the pigments content, chlorophylls a (30%), chlorophyll b (31%) and carotenoids (53%) were significantly reduced by thymol treatment, whereas that of anthocyanins was highly stimulated (64%) (Fig. 5).

3.6 Metabolomics

To get more insight into the effects of thymol on Arabidopsis metabolism, a GC/MS-driven untargeted-metabolomic analysis was carried out.

The multivariate analysis (PCA), carried on the annotated metabolites, highlighted a clear separation between two treatments, indicating that thymol induced significant alterations in

Arabidopsis metabolome. The separation was achieved using the principal components (PCs) PC1 *vs* PC2, which explained a total variance of 81.2 %. In particular, the PC1 and PC2 variables were responsible for 64.9 % and 16.3 % variation sources, respectively (Fig 6).

The loading plots analysis highlighted that the PC1 was mainly dominated by isothreonic acid, ethanolamine, tartaric acid, glycerol-3-phosphate and galactose, whereas the PC2 by galacturonic acid, inositol, sinigrin, ribose, methylmalonic acid and isoleucine (Fig 6 and S1).

Successively, data were analysed through univariate analysis and, based on t-test, the significant discriminating metabolites were identified (supplementary material S1).

Among them, eight amino acids, six organic acids, one oxidized vitamin and seven sugars have been annotated. Among the amino acids, β-alanine and threonine were the only ones significantly reduced by treatment (Table 1). On the contrary, proline, aspartic acid, glutamic acid, ornithine, serine and valine were significantly increased in response to thymol. A similar trend was observed also in organic acids, where malic acid was the only significantly inhibited, whereas all the others as well as the vitamin ascorbic acid increased in response to thymol (Table 1). Finally, among the sugars, sucrose and myo-inositol were significantly down-accumulated by treatment whereas galactinol, maltose, fructose, glucose and trehalose were up-accumulated (Table 1).

3.7 Proteomic analysis

A MS-based proteomic analysis was performed in *A. thaliana* plants following application of 300 μM thymol. Overall, the approach allowed annotating about 150 proteins passing the validation thresholds applied; the whole list of proteins is provided as supplementary material (supplementary material S2). The subsequent unsupervised hierarchical clustering identified two main sub-clusters, each of them including samples from the same treatment except for a thymol-treated sample that grouped with control (Figure 7). Notably, when looking at the fold-change based heat-map of the cluster analysis, several proteins showed a marked up-accumulation in response to the thymol treatment. Nonetheless, to note that this naïve analysis pointed out a relatively high biological variability within each treatment.

Thereafter, a subsequent supervised approach, namely PLS-DA analysis, was carried out using the treatment as class membership parameter. This further multivariate analysis confirmed that 300 μM thymol induced a distinct proteomic signature in *A. thaliana* plants (model accuracy: 100%) (supplementary materials S3). The most discriminant proteins were exported from PLS-DA covariance structures, according to their weight in the prediction model; these highly discriminant proteins are provided in table 1 together with their fold-change values. Consistently with the previous

analysis, most of proteins was accumulated following thymol application. Interestingly, all the down accumulated proteins were chloroplastic, such as ATP synthase, PSI or PSII proteins, as well as the chloroplastic phosphoglycerokinase 1. By contrast, the up accumulated proteins included, among the others, photosynthesis related proteins (such as CP43 chlorophyll apoprotein, plastocyanin, thylakoid lumenal 15kDa protein 1, probable plastid-lipid-associated protein 6 chloroplastic), ROS detoxification proteins (Probable peroxidase 26 and superoxide dismutase [Fe] 1 chloroplastic) and redox stress (plastid-lipid associated protein 6), proteins involved in fatty acids metabolism (ACP 4 and palmitoyl-ACP thioestherase) and in vacuole trafficking (V-type ATP-ase and vacuolar cation/proton exchanger). Noteworthy, ATP-synthase mitochondrial showed an opposite trend compared to its chloroplastic analogous.

Proteins passing the fold-change cut-off of 3 were also identified, in order to achieve more information on the proteome changes induced by thymol treatment (supplementary material S2). Differentially accumulated proteins were interpreted in both agriGO and DAVID for ontology analysis. The outcome of DAVID elaborations confirmed the involvement of chloroplast processes, with PSI, PSII and chlorophyll binding proteins being the most affected. Furthermore, the thioredoxin processes was also highlighted by this elaboration, further indicating the involvement of both photosynthesis and oxidative stress, also strongly confirmed by agriGO ontology.

4. Discussion

In the present study, the monoterpenic phenol thymol was screened by the *in-vitro* bioassays for its phytotoxicity on Arabidopsis seedlings. These rapid and cost-effective tools allowed to identify the key concentrations (Eg. ED_{50}, ED_{80} and/or LD_{50}) on which to focus the *in-situ* experiments in both laboratory and open fields (Araniti et al., 2017c). The results confirmed the high phytotoxic activity of this compound, already observed on other species (de Assis Alves et al., 2018; Nasrollahi et al., 2018), pointing out an ED_{50} value of 289 µM. For this reason, 300 µM thymol was later adopted to understand its mode of action on soilless cultured adult plants of *A. thaliana* by an integrated physiological, metabolomic and proteomic approach.

Our dataset clearly indicated that thymol strongly affected plant water status inducing a cascade effect starting from the ABA signal and stomatal closure. Consequently, a reduced evapotranspiration accompanied by an increment in leaf temperature followed by a ROS burst in leaves were observed, causing oxidative stress and cell membranes damages. The PSII efficiency was directly (physically damaged) or indirectly altered and this was translated in a strong reduction in plant growth and development. Taken together, these results suggested that thymol-treated plants were experiencing a

water status alteration followed by an oxidative damage, as already observed by Araniti et al. (2017b) and Graña et al. (2016) on Arabidopsis adult plants treated with the sesquiterpene *trans*-caryophyllene and the monoterpene citral, respectively. Below we detail the molecule mechanism by which thymol affected *A. thaliana* growth.

A significant decrease in leaf number and area, already after 4 days of treatment, accompanied by a reduction in both FW and DW were observed, suggesting an impairment in plant development triggered by thymol. Additionally, plants were characterized by a general decrease in protein content accompanied by a buildup in leaf osmotic potential, an increment in DW/FW ratio and a reduction in RWC.

In accordance with previous results in plants subjected to water status stress (Kuromori et al., 2018; Sharma and Rai, 1989) thymol treatment caused a significant increment in ABA content together with amino acids accumulation, responsible of stomata closure needed for reducing plant transpiration and water losses. Therefore, in plants treated with thymol, almost all the stomata on the leaf abaxial surface were closed, while the others showed a significant reduction in stomatal size and density. Doheny-Adams et al. (2012) reported that Arabidopsis plants exposed to drought developed stomata characterized by a reduced size. Smaller stomata not only provided a reduced total leaf pore area but allowed a faster aperture and closure response, maximizing the water use efficiency (Franks and Beerling, 2009; Drake et al., 2013; Lawson et al., 2014).

However, stomatal limitation contributed to a water conservation, limiting, at the same time, the influx of CO_2 to substomatal chamber and affecting the photosynthetic rate (Flexas and Medrano, 2002), as also observed in plants under drought stress condition (Bartlett et al., 2016).

Furthermore, a reduced water transpiration together with a prolonged stomatal closure lead to an increase of leaf temperature and, as a consequence, might promote ROS accumulation and physical damages to the photosynthetic machinery, especially to PSII, very sensitive to high temperature (Mathur and Jajoo, 2014). The thermal camera confirmed that, in thymol-treated plants, a significant higher temperature was measured particularly in the leaf blade margins, starting point of necrosis formation under drought stress (Vollenweider and Günthardt-Goerg, 2005; Vollenweider et al., 2016). In particular, leaf temperature lowered close to the petiole. Furthermore, in the leaf margins, the DAB staining highlighted a higher dark brown color (high concentration of H_2O_2), which gradually reduced its intensity moving towards the petiole. Similar results such as H_2O_2-induced lipid peroxidation and proteins content reduction were also observed in Arabidopsis leaves treated with the allelochemical 2-benzoxazolinone (Sánchez-Moreiras et al., 2011).

The ROS increase resulted in a perturbation of the cellular redox state that can ultimately lead to oxidative stress (Dumont and Rivoal, 2019). Proteomic results strongly supported the redox

imbalance in response to thymol treatment, which was indirectly suggested by the upregulation of the superoxide dismutase [Fe] 1 chloroplastic and PER26 (Probable peroxidase 26), that accumulated in response to oxidative stress to scavenge O_2^- and H_2O_2, respectively (Valèrio et al., 2004; Pilon et al., 2011). In particular, the PER26 enhancement may be related to the accumulation of oxidized ascorbate (dehydroascorbate) observed in treated plants, since this enzyme utilizes ascorbate as electron donor to scavenge H_2O_2.

Fold change analysis suggested that thymol treatment also affected the thioredoxin system, which plays an important role in redox homeostasis, since its catalytic site reduces disulphide bonds in target proteins thus affecting numerous biochemical processes (Kang et al., 2019). Furthermore, thioredoxin affected chloroplastic ATP-synthase acting as a switch under abiotic stresses (Carrillo et al., 2016). In chloroplast, the thioredoxin system includes also ferredoxin (Fd)-dependent thioredoxin reductase and reduced nicotinyl adenine dinucleoside phosphate NADPH-dependent thioredoxin reductase C(NTRC); this latter is known to regulate a wide diversity of biochemical processes including the redox signaling, the Calvin cycle, as well as the synthesis of starch and tetrapyrroles (Kang et al., 2019). Moreover, Vieira Dos Santos and Rei (2006) found that, under abiotic constrains, thioredoxin accumulation plays a key role in oxidative stress response. In agreement with our results, they identified peroxiredoxin and superoxide dismutase among the targets of thioredoxin, and postulated that the thioredoxin-induced cascade had a regulatory modulation of enzymes involved in repair and detoxication processes, thus offering a possible explanation to thymol-induced DNA damage.

A further link between thymol and ROS homeostasis has been related to its effects on salt overly signaling (SOS) pathway (Cheng et al., 2020), which is involved in Na^+/H^+ trafficking across membranes, including the vacuole. This might explain the accumulation of the vacuolar V-type ATP-ase and cation/proton exchanger, both involved in stress acclimation (Yokoi et al., 2002), observed in our results. A connection between the SOS signaling and ROS burst was also supported by the up-accumulation of the plastid -lipid associated protein 6, an osmiophilic transporter of antioxidants.

To maintain plant homeostasis and turgor and as well as to protect cells from ROS, plant responses to thymol were associated with an accumulation of several metabolites, such as, organic acids, sugars and sugar alcohols and amino acids. Data from the literature indicated that under oxidative stress complex changes in metabolite pools in central carbon metabolism (Dumont and Rivoal, 2019) with osmoprotectant function could be induced. In this respect, thymol treatments affected the tricarboxylic acid (TCA) cycle, which was significantly altered in both metabolomic and proteomic profiles. In particular, several Krebs cycle intermediates, such as citrate, fumarate, succinate and α-ketoglutarate, were significantly upregulated in response to thymol. These results were also in accordance with their role as key components in mechanisms useful to cope with environmental

stressors (Lopez-Bucio et al., 2000), such as thymol, or water stress (Timpa et al., 1986). In addition, some of these organic acids such as citric acid and fumaric acid ameliorated plant performances under stressful conditions, in particular enabling plant protection against ROS spread (El-Tohamy et al., 2013). In particular, fumarate, one of the major forms of fixed carbon in Arabidopsis (Chia et al., 2000), is converted to malate through a reversible hydration/dehydration catalysed by the enzyme fumarase (Fernie and Martinoia, 2009). Therefore, the reduction in malic acid observed in stressed plants could be due both to a reduction of fumarase activity or to a conversion of malate to fumarate in order to increase the availability of carbon skeletons and energy for the metabolization of other compounds to cope with stress (Chia et al., 2000). In particular, this second hypothesis was strongly supported by the experiments carried out by Kim and Lee (2002) who observed that in carrot cells, growing on malic acid as carbon source, it was firstly converted into fumaric acid by fumarase and then used for growth. Moreover, it has been proved that in Arabidopsis, a species which accumulates large amounts of fumarate, the malate is converted to fumarate by cytosolic fumarase (Pracharoenwattana et al., 2010), confirming the importance of this metabolite as source of carbon skeletons and the reduction on malate content under thymol stress. Finally, Nunes-Nesi et al. (2007) reported that a tomato mutant deficient in mitochondrial fumarase activity (low malate production) was characterized by a marked reduction of transpiration and stomatal conductance due to a deficiency in stomatal function, which is in line with our results.

In particular, the protein mitochondrial ATP synthase subunit d, which catalyzes the terminal step in oxidative respiration generating ATP, was significantly stimulated by the treatment. Zhang et al. (2008) reported that this protein isolated in Arabidopsis plants was able to confer resistance to several abiotic stress such as drought, cold and salinity.

Among the osmoprotective metabolites, proline, threalose and galactinol, the most effective compounds (Suprasanna et al. 2016), were significantly increased in thymol-treated plants. Interestingly, their biosynthesis is induced by both ABA signaling and metabolism (Sharma and Rai, 1989; Stewart and Voetberg, 1985; Taji et al., 2002; Yu et al., 2019). Furthermore, ABA in turn induced the enzyme galactinol synthase, which is involved in the biosynthesis of raffinose family oligosaccharides promoting plant stress tolerance (Nishizawa et al., 2008; Panikulangara et al., 2004; Taji et al., 2002).

Water status alteration and consequently stomatal limitation negatively affected photosynthesis, as demonstrated under mild to moderate drought conditions (Misson et al., 2010). Both DAVID and agriGO ontologies, gained from the differential proteins, highlighted that photosynthesis and chloroplastic processes were significantly affected by thymol treatment. Supportively, a high reduction in sucrose and in several proteins linked to photosynthesis together with a decrease of

pigments content supported this hypothesis. In particular, a reduction in both chlorophyll *a* and *b* as well as in carotenoids was observed in thymol-treatment plants. On the contrary, anthocyanins, which play a pivotal role in photoprotection, due to their sunscreen prerogative (Landi et al., 2015; Lo Piccolo et al., 2018), were significantly stimulated (0.7-fold higher than control) by thymol. Furthermore, the evaluation of several chlorophyll fluorescence parameters related to photosynthetic biochemistry activity, useful tool for monitoring the physiological status of the plant photosynthetic apparatus (Kalaji et al., 2016), confirmed the thymol effects on photosynthesis. In contrast with recent results on lettuce (Nasrollahi et al., 2018), the maximum photochemical efficiency of PSII (Fv/Fm) was significantly compromised by thymol treatment already after 6 days of treatment, while the other parameters (i.e. ϕ_{II}, ϕ_{NPQ}, ϕ_{NO}, qL and ETR) changed (were affected) from the 8th day onward. Undoubtedly, the duration of exposure to thymol, the concentrations applied and the diverse species between the experiments could contribute to this difference. The Fv/Fm decline denoted some damages to light harvesting complexes of PSII (LHCIIs) and PSII reaction centers (RCIIs). This decrease may be also related to the chlorophylls reduction (as observed in our experiment) as well as the denaturation of chlorophyll-binding proteins (Yamane et al.,1998), such as the antenna pigment-protein complex CP47 (Bricker and Frankel, 2002), down-regulated by thymol treatment. However, the up-regulation of CP43, pivotal for the light harvest by PSII (Bricker and Frankel, 2002), was not enough to preserve the impairment of PSII maximum quantum yield.

Beside damages to LHCII, a qL decrease, related to the closure of reaction centers, supported the occurrence of RCII damages induced by thymol treatment. This resulted in a lower ability of PSII to tunnel electrons to the photochemistry (lower ETR and yield of PSII under light-adapted conditions, namely ϕ_{II}). Similar results were observed by Graña et al. (2013; 2016) and Araniti et al. (2017b) on *Arabidopsis* adult plants treated with citral and coumarin, respectively.

Concerning the partitioning of harvested light in controlled and non-controlled dissipative mechanisms (Φ_{NPQ}, and Φ_{NO}, respectively), the stronger increase of both Φ_{NO} and Φ_{NPQ} values in thymol-treated plants reflected the sub-optimal capacity to photoprotect the photosynthetic apparatus (Klughammer et al., 2008). Indeed, Φ_{NO} usually reflects the fraction of energy that is passively dissipated in the form of heat and fluorescence, mainly due to the closed PSII, whereas Φ_{NPQ} corresponds to the fraction of energy dissipated in the form of heat *via* the regulated photoprotective NPQ mechanisms (Klughammer et al., 2008; Pfündel et al., 2008). The successful regulation in variable environmental stresses is generally aimed at maximal values of Φ_{PSII}, with the remaining loss 1-Φ_{PSII} aimed at a maximal ratio of Φ_{NPQ}/Φ_{NO} (Pfündel et al., 2008). At saturating light intensities, a stronger enhancement of non-regulated mechanisms can lead to photodamage and photoinhibition, in most cases shifting from dynamic to chronic photoinhibition.

In this context, the reduced photoprotective capacity of thymol-treated plants can be attributable to the lower carotenoids content. Indeed, carotenoids, in addition to their role of accessory pigments and as part of the dissipative NPQ, play an important role in protecting against photoinhibition acting as free radical scavengers (Choudhury and Behera, 2001; Demmig-Adams et al., 1996; Havaux and Kloppstech, 2001). Their strong reduction could have limited the protection against the photodegradation of chlorophyll, thereby facilitating the formation of ROS and increasing the possibility of photoinhibition (Havaux and Kloppstech, 2001; Hörtensteiner and Kräutler, 2011). Furthermore, we can postulate a contribution of the previously reported thioredoxin-mediated action, by thioredoxin reductase type C, acting on chlorophyll biosynthesis, on the impairment of photosynthetic processes.

The inability of thymol-treated plants to prevent photoinhibition and to protect PSII by photodegradation was also suggested by the down regulation of the chloroplastic ATP synthase subunit beta, which is involved in the production of ATP during the light dependent reaction. As summarized by Murata and Nishiyama (Murata and Nishiyama, 2018), the processes involved during the repair of photosystem II (PSII), experiencing photoinhibition, involves the replacement of photodamaged D1 protein by newly synthesized one. Both degradation and synthesis of D1 proteins during the repair of photosystem II are strictly dependent from the ATP produced by the chloroplastic ATP synthase. Furthermore, ATP is necessary for several other aspects involved in PSII repair, such as transcription of psbA genes, which encodes the precursor to D1 (pre-D1). These high requirements for ATP during the repair processes of PSII have been demonstrated by several authors, which showed that inhibitors of ATP synthase and uncouplers of ATP synthesis interrupt the biosynthesis of D1 and the repair of PSII.

Conclusions

In the present study thymol resulted a good candidate as a botanical herbicide, considering its high effectiveness on Arabidopsis plants.

The results strongly indicated that thymol caused an alteration of the plant water status that induced a cascade effect that started with ABA signalling and accumulation, and consequently a stomatal closure followed by a reduction of carbon absorption and metabolization. The reduction of evapotranspiration accompanied by the inability of the plants to fully dissipate the energy in excess induced an increase of leaf temperature at PSII level and a ROS burst, which reduced the membrane integrity andphysically damaged the photosynthetic machinery. Although thymol-treated plants tried to cope the stress, activating several enzymes involved in ROS detoxification and increasing the

concentrations of metabolites with osmoprotectants and sunscreen functions, the prolonged thymol treatment made plants unable to counteract the oxidative stress.

The present dataset offers a deep analysis on the biochemical and physiological mechanisms activated and/or repressed in Arabidopsis plants after thymol treatment and it encourages future research with the use of this molecule against weed species.

Founding

This research was supported by the Italian Ministry of Education, University and Research (MIUR), project SIR-2014 cod. RBSI14L9CE (MEDANAT).

Authors contribution

FA and MRA conceived and designed the study; FA performed physiological and metabolomic experiments, BMM and LL performed the proteomic analysis; FA, MRA, ML, BMM and LL analysed and interpreted the data. All the authors participated in manuscript development and writing. MRA did the final check and critical revision of the manuscript. FA funded the research.

Acknowledgement

A special thanks to Prof. Antonio Francesco Nucara (Dip. di Ingegneria Civile, dell'Energia, dell'Ambiente e dei Materiali, University mediterranea of Reggio Calabria) for making the images with the thermocamera.

Conflicts of interest

The authors declares no conflict of interest or disclosures.

Bibliography

Alipour, M., Saharkhiz, M.J., Niakousari, M., Damyeh, M.S., 2019. Phytotoxicity of encapsulated essential oil of rosemary on germination and morphophysiological features of amaranth and radish seedlings. Scientia Horticult. 243, 131-139.

Arancibia, M., Iler, D.C.I., Moreno-Toasa, G., & Rodriguez-Maecker, R.N., 2017. Thyme and rosemary essential oils as an alternative control of plant-parasitic nematodes. In Proceedings of MOL2NET 2016, International Conference on Multidisciplinary Sciences, 2nd edition MDPI, pp. 3900.

Araniti F., Graña E., Reigosa M.J., Sánchez-Moreiras A.M., Abenavoli MR., 2013. Individual and joint activity of terpenoids, isolated from *Calamintha nepeta* extract, on *Arabidopsis thaliana*. Nat. Prod. Res., 27(24), 2297-2303

Araniti, F., Bruno, L., Sunseri, F., Pacenza, M., Forgione, I., Bitonti, M.B., & Abenavoli, M.R., 2017a. The allelochemical farnesene affects *Arabidopsis thaliana* root meristem altering auxin distribution. Plant Physiol. Biochem., 121, 14-20.

Araniti, F., Grana, E., Krasuska, U., Bogatek, R., Reigosa, M.J., Abenavoli, M.R., Sanchez-Moreiras, A.M., 2016. Loss of gravitropism in farnesene-treated arabidopsis is due to microtubule malformations related to hormonal and ROS unbalance. PloS one, 11(8), e0160202.

Araniti, F., Lupini, A., Mauceri, A., Zumbo, A., Sunseri, F., Abenavoli, M.R., 2018. The allelochemical *trans*-cinnamic acid stimulates salicylic acid production and galactose pathway in maize leaves: a potential mechanism of stress tolerance. Plant Physiol. Biochem. 128, 32-40.

Araniti, F., Lupini, A., Sunseri, F., & Abenavoli, M.R., 2017b. Allelopatic potential of *Dittrichia viscosa* (L.) W. Greuter mediated by VOCs: a physiological and metabolomic approach. PloS one, 12(1), e0170161.

Araniti, F., Sánchez-Moreiras, A.M., Graña, E., Reigosa, M.J., Abenavoli, M.R., 2017c. Terpenoid *trans*-caryophyllene inhibits weed germination and induces plant water status alteration and oxidative damage in adult Arabidopsis. Plant Biol. 19(1), 79-89.

Araniti, F., Scognamiglio, M., Chambery, A., Russo, R., Esposito, A., D'Abrosca, B., Fiorentino, A., Lupini, A., Sunseri, F., Abenavoli, M.R., 2017d. Highlighting the effects of coumarin on adult plants of *Arabidopsis thaliana* (L.) Heynh. by an integrated-omic approach. J. Plant Physiol. 213, 30-41.

Bartlett, M.K., Klein, T., Jansen, S., Choat, B., Sack, L., 2016. The correlations and sequence of plant stomatal, hydraulic, and wilting responses to drought. P. Nat. A. Sci. 113(46), 13098-13103.

Belz, R.G., Hurle, K., Duke, S.O., 2005. Dose-response—a challenge for allelopathy?. Nonlinearity in biology, toxicology, medicine 3(2), nonlin-003.002. 002.

Benvenuti, S., Cioni, P.L., Flamini, G., Pardossi, A., 2017. Weeds for weed control: Asteraceae essential oils as natural herbicides. Weed Res. 57(5), 342-353.

Bernardo, L., Morcia, C., Carletti, P., Ghizzoni, R., Badeck, F.W., Rizza, F., Lucini, L., Terzi, V., 2017. Proteomic insight into the mitigation of wheat root drought stress by arbuscular mycorrhizae. J. Proteomics 169, 21-32.

Bradford, M.M., 1976. A rapid and sensitive method for the quantitation of microgram quantities of protein utilizing the principle of protein-dye binding. Anal. Biochem. 72(1-2), 248-254.

Bricker, T.M., Frankel, L.K., 2002. The structure and function of CP47 and CP43 in photosystem II. Photosyn. Res. 72(2), 131.

Busi, R., Goggin, D.E., Heap, I.M., Horak, M.J., Jugulam, M., Masters, R.A., Napier, R.M., Riar, D.S., Satchivi, N.M., Torra J. , Westra, P., 2018. Weed resistance to synthetic auxin herbicides. Pest Manag. Sci. 74(10), 2265-2276

Carrillo, L.R., Froehlich, J.E., Cruz, J.A., Savage, L.J., Kramer, D.M., 2016. Multi-level regulation of the chloroplast ATP synthase: the chloroplast NADPH thioredoxin reductase C (NTRC) is required for redox modulation specifically under low irradiance. Plant J. 87(6), 654-663.

Chen, C.J., Li, Q.Q., Ma, Y.N., Wang, W., Cheng, Y.X., Xu, F.R., Dong, X., 2019. Antifungal effect of essential oils from five kinds of Rutaceae plants–avoiding pesticide residue and resistance. Chem. Biodivers. 16(4), e1800688.

Cheng, Y.W., Kong, X.W., Wang, N., Wang, T.T., Chen, J., Shi, Z.Q., 2020. Thymol confers tolerance to salt stress by activating anti-oxidative defense and modulating Na^+ homeostasis in rice root. Ecotoxicol. Environm. Safety 188, 109894.

Chia, D.W., Yoder, T.J., Reiter, W.D., Gibson, S.I., 2000. Fumaric acid: an overlooked form of fixed carbon in Arabidopsis and other plant species. Planta 211(5), 743-751.

Chong, J., Soufan, O., Li, C., Caraus, I., Li, S., Bourque, G., Wishart, D.S., Xia, J., 2018. MetaboAnalyst 4.0: towards more transparent and integrative metabolomics analysis. Nucleic Acids Res. 46(W1), W486-W494.

Choudhury, N.K., Behera, R.K., 2001. Photoinhibition of photosynthesis: role of carotenoids in photoprotection of chloroplast constituents. Photosynthetica 39(4), 481-488.

de Assis Alves, T., Pinheiro, P.F., Praça-Fontes, M.M., Andrade-Vieira, L.F., Corrêa, K.B., de Assis Alves, T., da Cruz, F.A., Júnior, V.L., Ferreira, A., Soares, T.C.B., 2018. Toxicity of thymol, carvacrol and their respective phenoxyacetic acids in *Lactuca sativa* and *Sorghum bicolor*. Ind. Crops Prod. 114, 59-67.

Demmig-Adams, B., Adams III, W. W., Barker, D.H., Logan, B.A., Bowling, D.R., Verhoeven, A.S., 1996. Using chlorophyll fluorescence to assess the fraction of absorbed light allocated to thermal dissipation of excess excitation. Physiol. Plantarum 98(2), 253-264.

Doheny-Adams, T., Hunt, L., Franks, P.J., Beerling, D.J., Gray, J.E., 2012. Genetic manipulation of stomatal density influences stomatal size, plant growth and tolerance to restricted water supply across a growth carbon dioxide gradient. Philosophical Transactions of the Royal Society B: Biol. Sci. 367(1588), 547-555.

Dos Santos, C.V., Rey, P., 2006. Plant thioredoxins are key actors in the oxidative stress response. Trends Plant Sci. 11(7), 329-334.

Drake, P.L., Froend, R.H., Franks, P.J., 2013. Smaller, faster stomata: scaling of stomatal size, rate of response, and stomatal conductance. J. Exp. Bot. 64(2), 495-505.

Duke, S.O., Owens, D.K., Dayan, F.E., 2018. Natural product-based chemical herbicides, weed control: sustainability, hazards, and risks in cropping systems worldwide; Korres, NE, Burgos, NR, Duke, SO, Eds, 53-165.

Dumont, S., Rivoal, J., 2019. Consequences of oxidative stress on plant glycolytic and respiratory metabolism. Frontiers Plant Sci. 10, 166.

El-Tohamy, W.A., El-Abagy, H.M., Badr, M.A., Gruda, N., 2013. Drought tolerance and water status of bean plants (*Phaseolus vulgaris* L.) as affected by citric acid application. J. Appl. Bot. Food Qual. 86(1).

Fernie, A.R., Martinoia, E., 2009. Malate. Jack of all trades or master of a few?. Phytochem. 70(7), 828-832.

Flexas, J., Medrano, H., 2002. Drought-inhibition of photosynthesis in C3 plants: stomatal and non-stomatal limitations revisited. Ann. Bot. 89(2), 183-189.

Franks, P.J., Beerling, D.J., 2009. Maximum leaf conductance driven by CO_2 effects on stomatal size and density over geologic time. P. Nat. A. Sci. 106(25), 10343-10347.

Galperin, M.Y., Cochrane, G.R., 2009. Nucleic acids research annual database issue and the NAR online molecular biology database collection in 2009. Nucleic Acids Res. 37(suppl_1), D1-D4.

Giusti, M.M., Wrolstad, R.E., 2001. Characterization and measurement of anthocyanins by UV-visible spectroscopy. Curr. Prot. Food Anal. Chem. (1), F1. 2.1-F1. 2.13.

González L., 2001. Determination of water potential in leaves. In Handbook of plant ecophysiology techniques (pp. 193-205). Springer, Dordrecht.

González, L., & González-Vilar, M. (2001). Determination of relative water content. In Handbook of plant ecophysiology techniques (pp. 207-212). Springer, Dordrecht.

Graña, E., Díaz-Tielas, C., López-González, D., Martínez-Peñalver, A., Reigosa, M.J., Sánchez-Moreiras, A.M., 2016. The plant secondary metabolite citral alters water status and prevents seed formation in *Arabidopsis thaliana*. Plant Biol. 18(3), 423-432.

Graña, E., Sotelo, T., Díaz-Tielas, C., Araniti, F., Krasuska, U., Bogatek, R., Reigosa, M.J., Sánchez-Moreiras, A. M., 2013. Citral induces auxin and ethylene-mediated malformations and arrests cell division in *Arabidopsis thaliana* roots. J. Chem. Ecol., 39(2), 271-282.

Graña, E., Sotelo, T., Díaz-Tielas, C., Reigosa, M.J., Sánchez-Moreiras, A.M., 2013. The phytotoxic potential of the terpenoid citral on seedlings and adult plants. Weed Sci. 61(3), 469-481.

Gursul, S., Karabulut, I., & Durmaz, G., 2019. Antioxidant efficacy of thymol and carvacrol in microencapsulated walnut oil triacylglycerols. Food Chem. 278, 805-810.

Harrison, S.K., & Loux, M.M., 2017. Chemical weed management. In Handbook of weed management systems (pp. 101-153). Routledge.

Havaux, M., Kloppstech, K., 2001. The protective functions of carotenoid and flavonoid pigments against excess visible radiation at chilling temperature investigated in Arabidopsis npq and tt mutants. Planta 213(6), 953-966.

Hodges, D.M., DeLong, J.M., Forney, C.F., Prange, R.K., 1999. Improving the thiobarbituric acid-reactive-substances assay for estimating lipid peroxidation in plant tissues containing anthocyanin and other interfering compounds. Planta 207(4), 604-611.

Horai, H., Arita, M., Kanaya, S., Nihei, Y., Ikeda, T., Suwa, K., Ojima, Y., Tanaka, K., Tanaka, S., Aoshima, K., Oda, Y., 2010. MassBank: a public repository for sharing mass spectral data for life sciences. J. Mass Spec. 45(7), 703-714.

Hörtensteiner, S., Kräutler, B., 2011. Chlorophyll breakdown in higher plants. Biochimica et Biophysica Acta (BBA)-Bioenergetics 1807(8), 977-988.

Isman, M.B., 2019. Commercial development of plant essential oils and their constituents as active ingredients in bioinsecticides. Phytochem. Rev. 1-7.

Kalaji, H. M., Jajoo, A., Oukarroum, A., Brestic, M., Zivcak, M., Samborska, I.A., Cetner, M.D., Łukasik, I., Goltsev, V., Ladle, R.J., 2016. Chlorophyll a fluorescence as a tool to monitor physiological status of plants under abiotic stress conditions. Acta Physiol. Plantarum 38(4), 102.

Kang, Z., Qin, T., Zhao, Z., 2019. Thioredoxins and thioredoxin reductase in chloroplasts: A review. Gene 32-42.

Kim, S., Lee, W., 2002. Participation of extracellular fumarase in the utilization of malate in cultured carrot cells. Plant Cell Rep. 20(11), 1087-1092.

Klughammer, C., Schreiber, U., 2008. Complementary PS II quantum yields calculated from simple fluorescence parameters measured by PAM fluorometry and the Saturation Pulse method. PAM application notes 1(2), 201-247.

Kopka, J., Schauer, N., Krueger, S., Birkemeyer, C., Usadel, B., Bergmüller, E., Dörmann, P., Weckwerth, W., Gibon, Y., Willmitzer, L., 2005. GMD@ CSB. DB: the Golm metabolome database. Bioinformatics 21(8), 1635-1638.

Kordali, S., Cakir, A., Ozer, H., Cakmakci, R., Kesdek, M., Mete, E., 2008. Antifungal, phytotoxic and insecticidal properties of essential oil isolated from Turkish *Origanum acutidens* and its three components, carvacrol, thymol and p-cymene. Biores. Technol. 99(18), 8788-8795.

Kuromori, T., Seo, M., Shinozaki, K., 2018. ABA transport and plant water stress responses. Trends Plant Sci. 23(6), 513-522.

Landi, M., 2017. Commentary to:“Improving the thiobarbituric acid-reactive-substances assay for estimating lipid peroxidation in plant tissues containing anthocyanin and other interfering compounds” by Hodges et al., Planta (1999) 207: 604–611. Planta 245(6), 1067-1067.

Landi, M., Araniti, F., Flamini, G., Piccolo, E. L., Trivellini, A., Abenavoli, M.R., Guidi, L., 2020. "Help is in the air": volatiles from salt-stressed plants increase the reproductive success of receivers under salinity. Planta, 251(2), 1-15.

Landi, M., Tattini, M., Gould, K.S., 2015. Multiple functional roles of anthocyanins in plant-environment interactions. Environ. Exp. Bot. 119, 4-17.

Lawson, T., Simkin, A.J., Kelly, G., Granot, D., 2014. Mesophyll photosynthesis and guard cell metabolism impacts on stomatal behaviour. New Phytol. 203(4), 1064-1081.

Li, Y., Wen, J. M., Du, C.J., Hu, S.M., Chen, J.X., Zhang, S.G., Gao, F., Li, S.J., Mao, X.W., Miyamoto, H., 2017. Thymol inhibits bladder cancer cell proliferation via inducing cell cycle arrest and apoptosis. Biochem. Biophys. Res. Comm. 491(2), 530-536.

Lisec, J., Schauer, N., Kopka, J., Willmitzer, L., Fernie, A.R., 2006. Gas chromatography mass spectrometry–based metabolite profiling in plants. Nature Prot. 1(1), 387.

Lo Piccolo, E., Landi, M., Pellegrini, E., Agati, G., Giordano, C., Giordani, T., Lorenzini, G., Malorgio, F., Massai, R., Rallo, G., 2018. Multiple consequences induced by epidermally-located anthocyanins in young, mature and senescent leaves of Prunus. Frontiers Plant Sci. 9, 917.

Lopez-Bucio, J., Nieto-Jacobo, M.F., Ramırez-Rodrıguez, V., Herrera-Estrella, L., 2000. Organic acid metabolism in plants: from adaptive physiology to transgenic varieties for cultivation in extreme soils. Plant Sci. 160(1), 1-13.

Malone, S.R., Mayeux, H.S., Johnson, H.B., Polley, H.W., 1993. Stomatal density and aperture length in four plant species grown across a subambient CO_2 gradient. American J. Bot. 80(12), 1413-1418.

Martínez-Peñalver A., Reigosa M.J., Sánchez-Moreiras A.M., 2011. Imaging chlorophyll *a* fluorescence reveals specific spatial distributions under different stress conditions. Flora-Morphology, Distribution, Functional Ecology of Plants, 206(9), 836-844.

Mathur, S., Jajoo, A., 2014. Alterations in photochemical efficiency of photosystem II in wheat plant on hot summer day. Physiol. Molecul. Biol. Plants 20(4), 527-531.

Matković, A., Marković, T., Vrbničanin, S., Sarić-Krsmanović, M., Božić, D., 2018. Chemical composition and in vitro herbicidal activity of five essential oils on Johnson grass (*Sorghum halepense* [L.] Pers.). Lekovite sirovine 38, 44-50.

Misson, L., Limousin, J.M., Rodriguez, R., Letts, M.G., 2010. Leaf physiological responses to extreme droughts in Mediterranean *Quercus ilex* forest. Plant Cell Environ. 33(11), 1898-1910.

Murata, N., Nishiyama, Y., 2018. ATP is a driving force in the repair of photosystem II during photoinhibition. Plant Cell Environ. 41(2), 285-299.

Naghdi Badi, H., Abdollahi, M., Mehrafarin, A., Ghorbanpour, M., Tolyat, M., Qaderi, A., Ghiaci Yekta, M., 2017. An overview on two valuable natural and bioactive compounds, thymol and carvacrol, in medicinal plants. J. Med. Plants 3(63), 1-32.

Nasrollahi, P., Razavi, S.M., Ghasemian, A., Zahri, S., 2018. Physiological and biochemical responses of lettuce to thymol, as allelochemical. Russian J. Plant Physiol. 65(4), 598-603.

Nikolova, M.T., & Berkov, S.H., 2018. Use of essential oils as natural herbicides. Ecologia Balkanica, 10(2).

Nishizawa, A., Yabuta, Y., Shigeoka, S., 2008. Galactinol and raffinose constitute a novel function to protect plants from oxidative damage. Plant Physiol. 147(3), 1251-1263.

Nunes-Nesi, A., Carrari, F., Gibon, Y., Sulpice, R., Lytovchenko, A., Fisahn, J., Graham, J., Ratcliffe, R.G., Sweetlove, L.J., Fernie, A.R., 2007. Deficiency of mitochondrial fumarase activity in tomato plants impairs photosynthesis via an effect on stomatal function. Plant J. 50(6), 1093-1106.

Panikulangara, T.J., Eggers-Schumacher, G., Wunderlich, M., Stransky, H., Schöffl, F., 2004. Galactinol synthase1. A novel heat shock factor target gene responsible for heat-induced synthesis of raffinose family oligosaccharides in Arabidopsis. Plant Physiol. 136(2), 3148-3158.

Pfündel, E., Klughammer, C., Schreiber, U., 2008. Monitoring the effects of reduced PS II antenna size on quantum yields of photosystems I and II using the Dual-PAM-100 measuring system. PAM Application Notes 1, 21-24.

Pilon, M., Ravet, K., Tapken, W., 2011. The biogenesis and physiological function of chloroplast superoxide dismutases. Biochimica et Biophysica Acta (BBA)-Bioenergetics 1807(8), 989-998.

Pivetta, T.P., Simões, S., Araújo, M.M., Carvalho, T., Arruda, C., Marcato, P.D., 2018. Development of nanoparticles from natural lipids for topical delivery of thymol: Investigation of its anti-inflammatory properties. Colloids and Surfaces B: Biointerfaces 164, 281-290.

Pracharoenwattana, I., Zhou, W., Keech, O., Francisco, P.B., Udomchalothorn, T., Tschoep, H., Stitt, M., Gibon, Y., Smith, S. M., 2010. Arabidopsis has a cytosolic fumarase required for the massive allocation of photosynthate into fumaric acid and for rapid plant growth on high nitrogen. Plant J. 62(5), 785-795.

Radoglou, K.M., Jarvis, P.G., 1990. Effects of CO2 enrichment on four poplar clones. I. Growth and leaf anatomy. Ann. Bot. 65(6), 617-626.

Rawlinson, C., Kamphuis, L.G., Gummer, J.P., Singh, K.B., Trengove, R.D., 2015. A rapid method for profiling of volatile and semi-volatile phytohormones using methyl chloroformate derivatisation and GC–MS. Metabolomics 11(6), 1922-1933.

Sairam R.K., Rao K.V., Srivastava G., 2002. Differential response of wheat genotypes to long term salinity stress in relation to oxidative stress, antioxidant activity and osmolyte concentration. Plant

Sci. 163(5), 1037–46. Salehi, B., Mishra, A.P., Shukla, I., Sharifi-Rad, M., Contreras, M.D.M., Segura-Carretero, A., Fathi, H., Nasrabadi, N.N., Kobarfard, F., Sharifi-Rad, J., 2018. Thymol, thyme, and other plant sources: Health and potential uses. Phytotherapy Res. 32(9), 1688-1706.

Salehi, H., Chehregani, A., Lucini, L., Majd, A., Gholami, M., 2018. Morphological, proteomic and metabolomic insight into the effect of cerium dioxide nanoparticles to *Phaseolus vulgaris* L. under soil or foliar application. Sci. Tot. Environ. 616, 1540-1551.

Sánchez-Moreiras, A.M., Martínez-Peñalver, A., Reigosa, M.J., 2011. Early senescence induced by 2-3H-benzoxazolinone (BOA) in *Arabidopsis thaliana*. J. Plant Physiol. 168(9), 863-870.

Sharma, U.D., Rai, V.K., 1989. Modulation of osmotic closure of stomata, stomatal resistance and K^+ fluxes by exogenous amino acids in *Vicia faba* L. leaves. Biochem. Physiol. Pfl. 185(5-6), 369-376.

Sherman, B.T., Lempicki, R.A., 2009. Systematic and integrative analysis of large gene lists using DAVID bioinformatics resources. Nat. Prot. 4(1), 44.

Stewart, C.R., Voetberg, G., 1985. Relationship between stress-induced ABA and proline accumulations and ABA-induced proline accumulation in excised barley leaves. Plant Physiol. 79(1), 24-27.

Suprasanna, P., Nikalje, G.C., Rai, A.N., 2016. Osmolyte accumulation and implications in plant abiotic stress tolerance. In Osmolytes and plants acclimation to changing environment: Emerging omics technologies (pp. 1-12). Springer, New Delhi.

Taji, T., Ohsumi, C., Iuchi, S., Seki, M., Kasuga, M., Kobayashi, M., Yamaguchi-Shinozaki, K., Shinozaki, K., 2002. Important roles of drought-and cold-inducible genes for galactinol synthase in stress tolerance in *Arabidopsis thaliana*. Plant J. 29(4), 417-426.

Tian, T., Liu, Y., Yan, H., You, Q., Yi, X., Du, Z., Xu, W., Su, Z., 2017. agriGO v2. 0: a GO analysis toolkit for the agricultural community, 2017 update. Nucleic Acids Res. 45(W1), W122-W129.

Timpa, J. D., Burke, J.J., Quisenberry, J.E., Wendt, C.W., 1986. Effects of water stress on the organic acid and carbohydrate compositions of cotton plants. Plant Physiol. 82(3), 724-728.

Tsugawa, H., Cajka, T., Kind, T., Ma, Y., Higgins, B., Ikeda, K., Kanazawa, M., VanderGheynst, J., Fiehn, O., Arita, M., 2015. MS-DIAL: data-independent MS/MS deconvolution for comprehensive metabolome analysis. Nat. Meth. 12(6), 523.

Valério, L., De Meyer, M., Penel, C., Dunand, C., 2004. Expression analysis of the Arabidopsis peroxidase multigenic family. Phytochem. 65(10), 1331-1342.

van Acker F.A., Schouten O., Haenen G.R., van der Vijgh W.J., Bast A., 2000. Flavonoids can replace α-tocopherol as an antioxidant. FEBS let. 473(2), 145-148

Vollenweider, P., Günthardt-Goerg, M. S., 2005. Diagnosis of abiotic and biotic stress factors using the visible symptoms in foliage. Environ. Pollution 137(3), 455-465.

Vollenweider, P., Menard, T., Arend, M., Kuster, T.M., Günthardt-Goerg, M.S., 2016. Structural changes associated with drought stress symptoms in foliage of Central European oaks. Trees 30(3), 883-900.

Wellburn, R.W., 1994. The spectral determination of chlorophylls a and b, as well as total carotenoids, using various solvents with spectrophotometers of different resolution. J. Plant Physiol. 144(3), 307-313.

Westwood, J.H., Charudattan, R., Duke, S.O., Fennimore, S.A., Marrone, P., Slaughter, D.C., Swanton, C., Zollinger, R., 2018. Weed management in 2050: perspectives on the future of weed science. Weed Sci. 66(3), 275-285.

Xu, Z., Zhou, G., 2008. Responses of leaf stomatal density to water status and its relationship with photosynthesis in a grass. J. Exp. Bot. 59(12), 3317-3325.

Yamane, Y., Kashino, Y., Koike, H., Satoh, K., 1998. Effects of high temperatures on the photosynthetic systems in spinach: oxygen-evolving activities, fluorescence characteristics and the denaturation process. Photosyn. Res. 57(1), 51-59.

Yokoi, S., Quintero, F.J., Cubero, B., Ruiz, M.T., Bressan, R.A., Hasegawa, P.M., Pardo, J. M., 2002. Differential expression and function of *Arabidopsis thaliana* NHX Na^+/H^+ antiporters in the salt stress response. Plant J. 30(5), 529-539.

Yu, W., Zhao, R., Wang, L., Zhang, S., Li, R., Sheng, J., Shen, L., 2019. ABA signaling rather than ABA metabolism is involved in trehalose-induced drought tolerance in tomato plants. Planta 250(2), 643-655.

Zhang, X., Liu, S., Takano, T., 2008. Overexpression of a mitochondrial ATP synthase small subunit gene (AtMtATP6) confers tolerance to several abiotic stresses in *Saccharomyces cerevisiae* and *Arabidopsis thaliana*. Biotechnol. Letters 30(7), 1289-1294.

Zimdahl, R.L., 2018. Fundamentals of weed science. Academic press.

Zunino, M.P., Zygadlo, J.A., 2005. Changes in the composition of phospholipid fatty acids and sterols of maize root in response to monoterpenes. J. Chem. Ecol. 31(6), 1269-1283

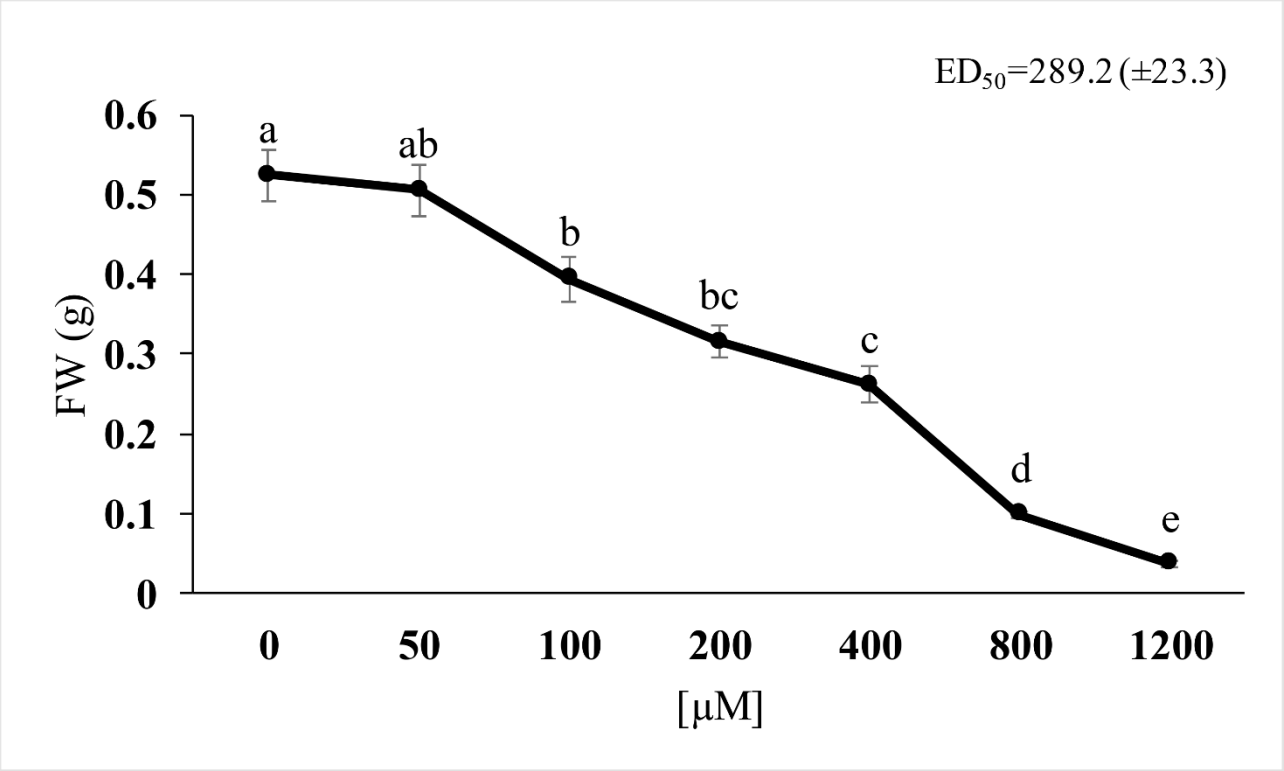

Figure 1: Non-linear regression fit of the dose-response curve calculated on shoot fresh weight of Arabidopsis seedlings treated with thymol 0-1200 µM for 14 days. N=4.

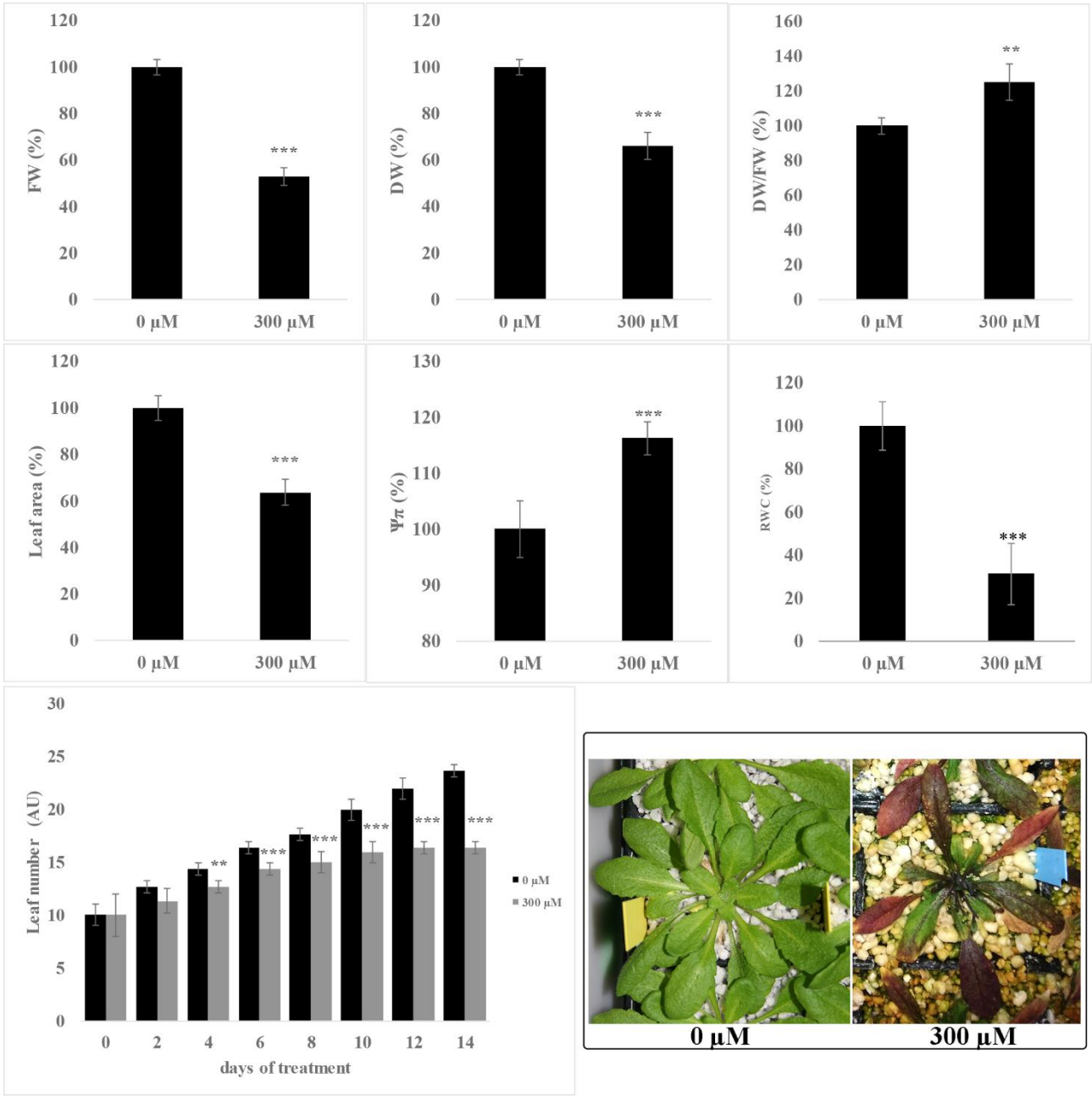

Figure 2: Fresh weight (FW), dry weight (DW), DW/FW, leaf area and number, osmotic potential (Ψπ), relative water content (RWC) and plant growth and development comparison between treated and untreated plants (Photo). Data are expressed as percentage compared to control. Asterisks indicate significant differences between mean values of treated and control plants after *t*-test with $P \leq 0.05$: * ($P \leq 0.05$), ** ($P \leq 0.01$), *** ($P \leq 0.001$). N=4.

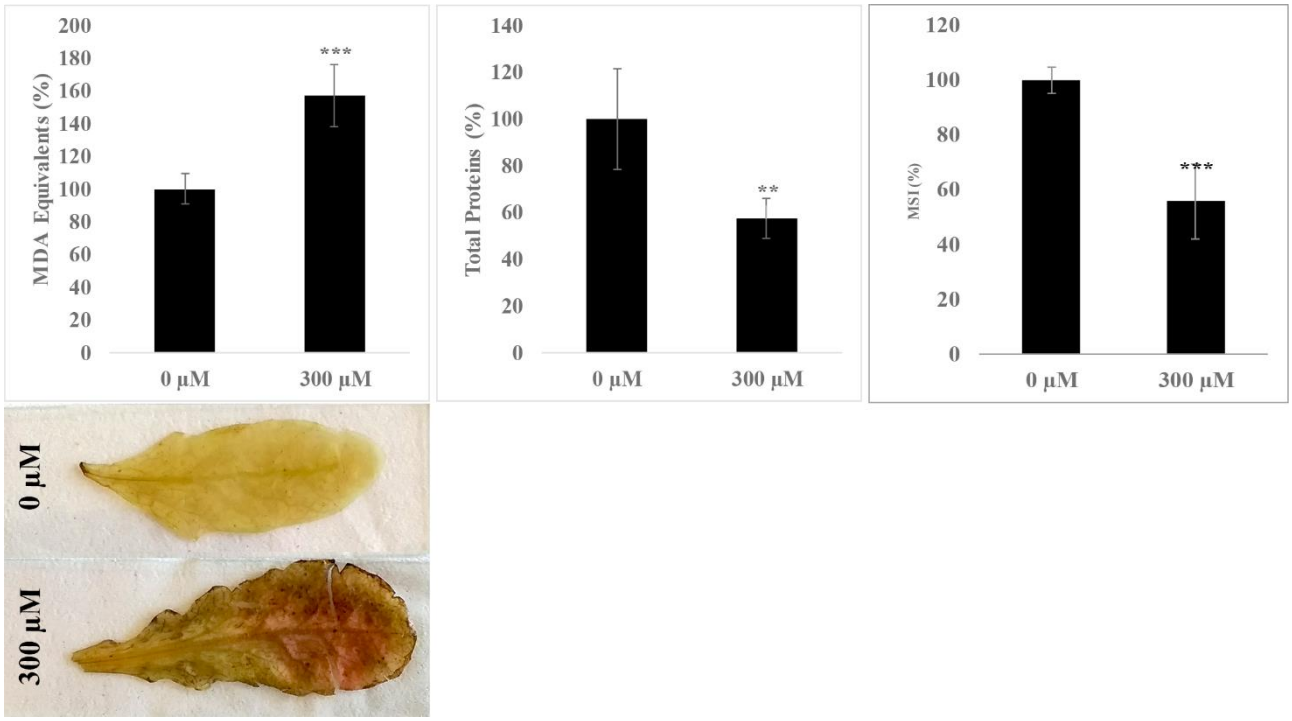

Figure 3: Lipid peroxidation, total proteins content, membrane stability index (MSI and *in-situ* semi-quantitative determination of H_2O_2 evaluated on *Arabidopsis* plants exposed to thymol (0 and 300 µM) (Photo). Data are expressed as percentage compared to control. Asterisks indicate significant differences between mean values of treated and control plants after *t*-test with $P \leq 0.05$: * ($P \leq 0.05$), ** ($P \leq 0.01$), *** ($P \leq 0.001$). N=4.

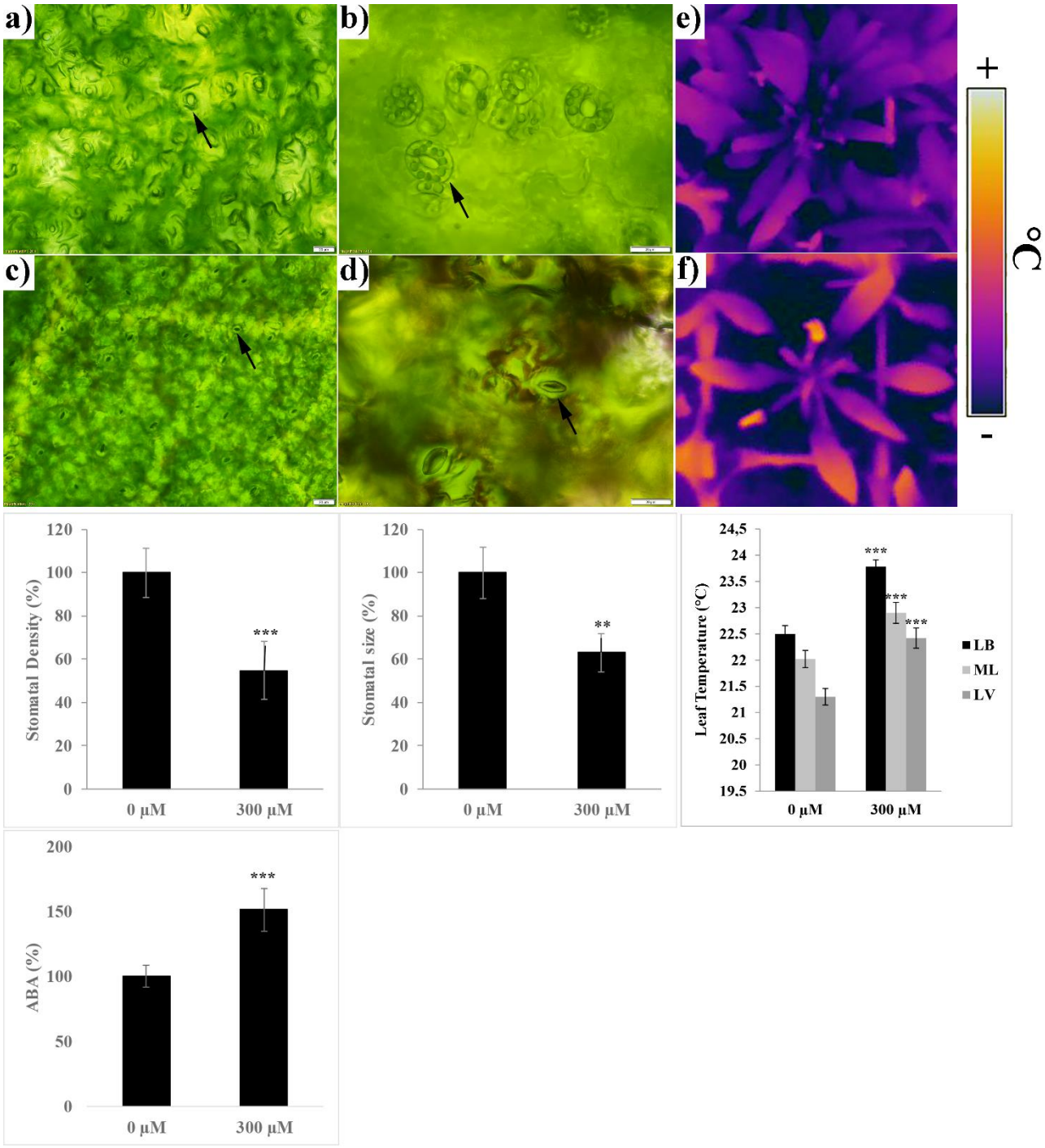

Figure 4: In the following image are reported: Imaging of stomata in untreated (a-b) and treated (c-d) plants. Thermocamera images reporting the changes in temperature in both untreated (e) and thymol-treated (f) plants. Moreover the effects of thymol on stomatal size and density, leaf temperature along leaf blade (LB, leaf blade border ; ML, middle leaf blade ; and LV, leaf vein and petiole) and abscisic acid (ABA) content.

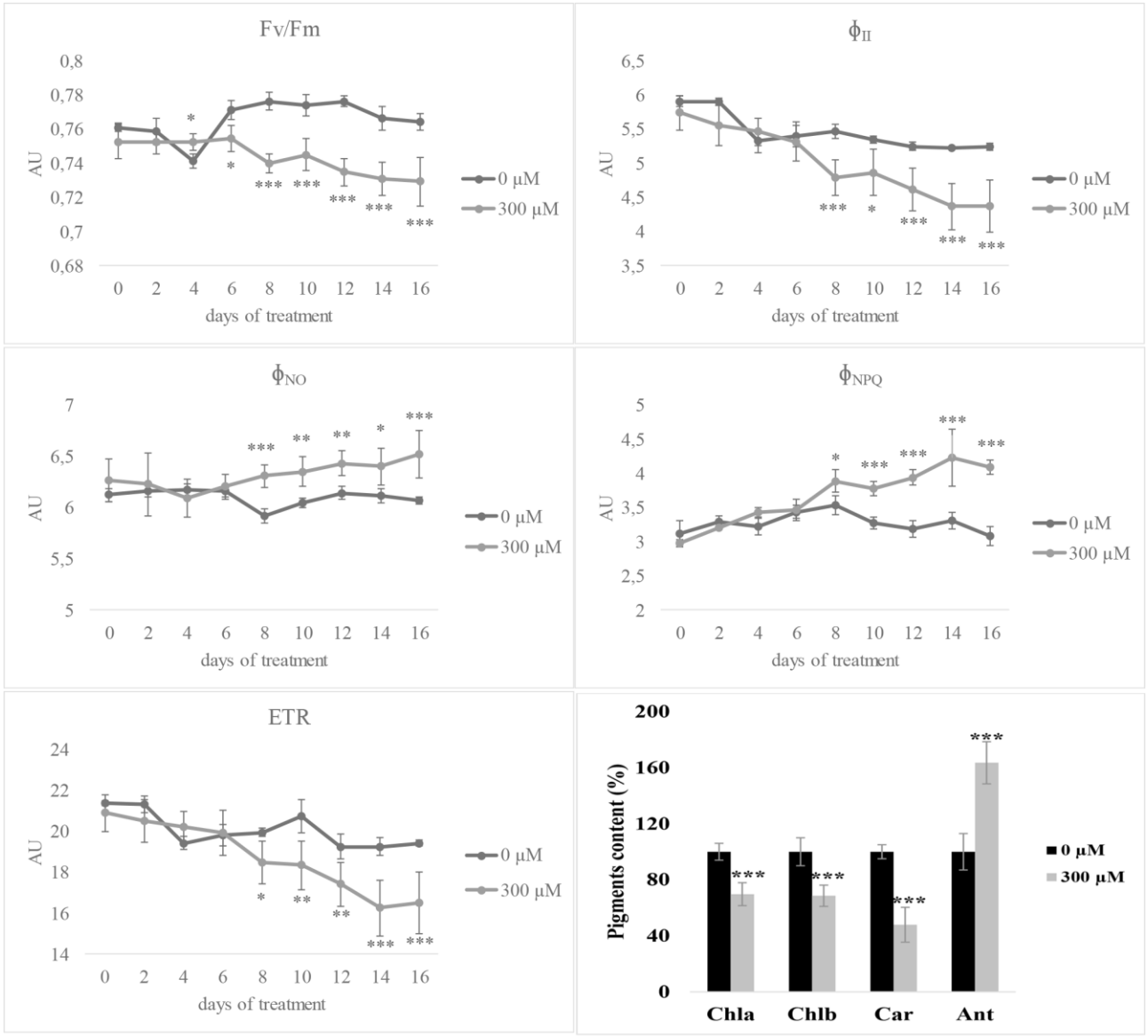

Figure 5: Values of maximum quantum efficiency of photosystem II (PSII) in dark-adapted conditions (F_v/F_m), PSII operating efficiency (ϕ_{II}), quantum yield of regulated (ϕ_{NPQ}) and nonregulated energy dissipation of PSII (ϕ_{NO}), apparent electron transport rate (ETR), Estimates the fraction of open PSII

centres (qL) and pigments content in *Arabidopsis* seedlings exposed to thymol (300 µM). Measurements were carried out every two days from the beginning (day 0) till the end (day 10) of the treatment. Fifteen measures were obtained for each parameter at each measuring time, which gave a kinetic plot for each parameter along the time. The integral value of the area was obtained from for each parameter at every time. * $P < 0.05$; ** $P < 0.01$; *** $P < 0.001$. AU = Arbitrary Units. Chlorophyll a fluorescence, N=3. Pigments content, N=4.

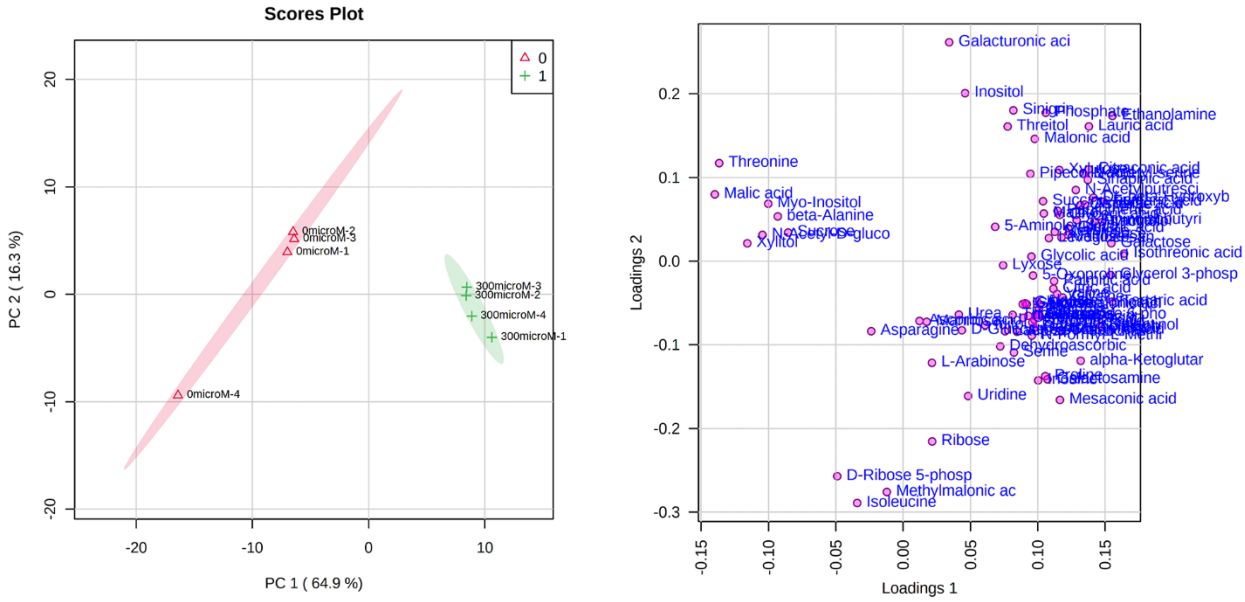

Figure 6. PCA analysis carried on the metabolite identified and quantified after thymol (300 µM) treatment. Principal Component analysis model scores **A)** and loading plot **B)** of metabolite profile of untreated (0 µM) and treated plants (300 µM). Both score and loading plots were generated using the first two PCs, PC1 *vs* PC2, with the explained variances shown in brackets.

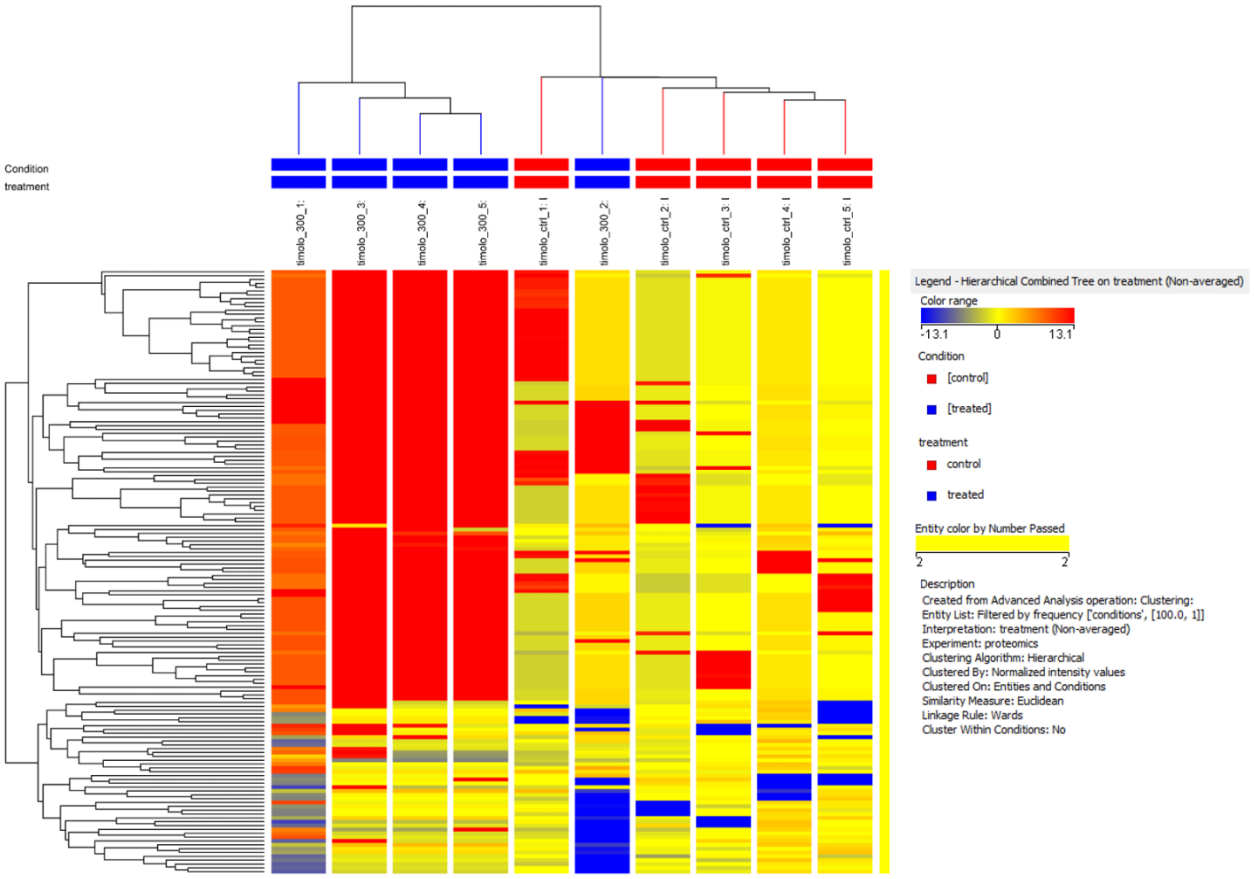

Figure 7: Hierarchical cluster analysis (distance: Euclidean, linkage rule: Ward's) carried out from proteomic profile of *A. thaliana* treated with 300 µM thymol, compared to control.

Table 1: Effects of thymol treatment (300 µM) on metabolite content.

Metabolites	0 µM	300 µM	Classes
beta-Alanine	2.84 (±0.21)	0.746 (±0.08)***	**Amino acids**
Proline	0.022 (±0.01)	0.177 (±0.07)**	
Threonine	0.196 (±0.02)	0.015 (±0.01)*	
Aspartate	0.018 (±0.01)	0.116 (±0.02)*	
Glutamate	0.0015 (±0.0002)	0.0139 (±0.004)***	
Ornithine	0.013 (±0.01)	0.079 (±0.02)*	
Serine	0.006 (±0.002)	0.021 (±0.009)**	
Valine	0.0003 (±0.0001)	0.002 (±0.0007)**	
5-Oxoproline	0.0037 (±0.001)	0.012 (±0.001)**	**Amino acid derivative**
Fumaric acid	0.239 (±0.16)	2.313 (±0.27)*	**Organic acids**
Citric acid	0.005 (±0.002)	0.026 (±0.004)**	
α-Ketoglutaric acid	0.035 (±0.01)	0.647 (±0.32)***	
Succinic acid	0.005 (±0.003)	0.015 (±0.004)*	
Malic acid	1.090 (±0.14)	0.053 (±0.02)***	
Dehydroascorbate	0.045 (±0.015)	0.127 (±0.024)**	**Oxidized vitamin**
Threonic acid	0.02 (±0.01)	0.068 (±0.015)*	**Carboxy acids**
Maltose	0.036 (±0.02)	0.18 (±0.02)**	**Sugars**
Glucose	0.348 (±0.013)	1.284 (±0.14)***	
Fructose	3.11 (±0.74)	13.97 (±0.95)***	
Sucrose	1.46 (±0.19)	0.468 (±0.16)**	
Trehalose	0.21 (±0.11)	1.22 (±0.08)**	
Galactinol	1.55 (±0.18)	36.19 (±3.11)***	**Polyols**
Myo-Inositol	0.54 (±0.06)	0.012 (±0.02)***	

Data are expressed as peak intensity normalized in comparison to the internal standard ribitol. Values in brackets indicate Standard Deviation. Statistical significance of the data was evaluated through *t*-Test with $P \leq 0.05$. N=4.